Cell Reports

Article

Mitochondrial biogenesis in developing astrocytes regulates astrocyte maturation and synapse formation

Graphical abstract

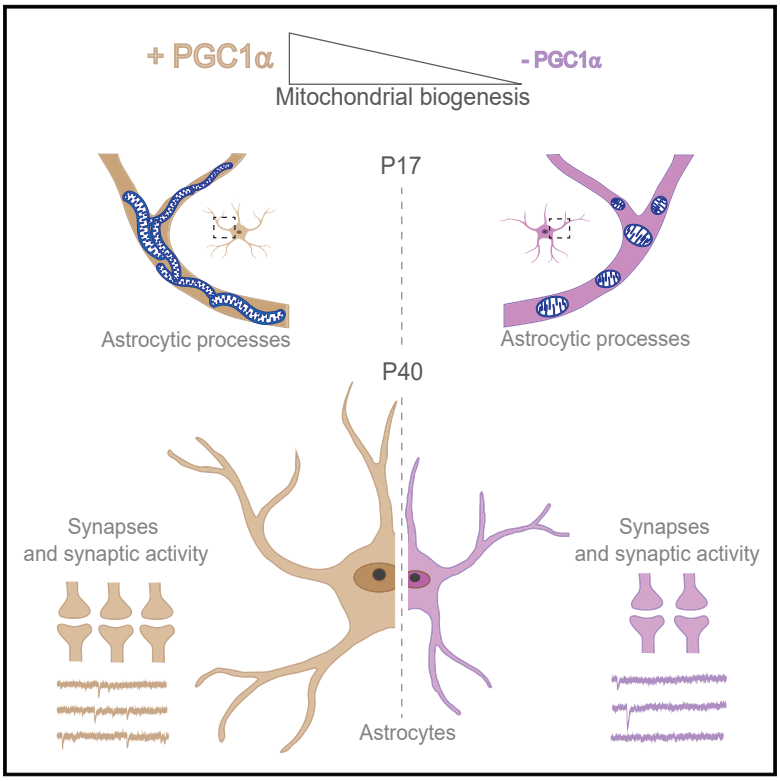

Authors

Tamara Zehnder, Francesco Petrelli, Jennifer Romanos, ..., Franck Polleux, Mirko Santello, Paola Bezzi

Correspondence

mirko.santello@pharma.uzh.ch (M.S.), paola.bezzi@unil.ch (P.B.)

In brief

Zehnder et al. demonstrate that proper levels of PGC-1α are necessary to induce a correct mitochondrial biogenesis in developing astrocytes and, consequently, to coordinate post-natal astrocyte morphogenesis and synaptogenesis.

Highlights

- Developing astrocytes contain a highly interconnected functional network of mitochondria
- Mitochondrial biogenesis in developing astrocytes is controlled by PGC-1α
- mGluR5 signaling modulates PGC-1α levels in developing astrocytes
- Deletion of PGC1-1α and mGluR5 impairs astrocyte maturation and synaptogenesis

Zehnder et al., 2021, Cell Reports *35*, 108952
April 13, 2021
https://doi.org/10.1016/j.celrep.2021.108952

CellPress

Cell Reports

CellPress
OPEN ACCESS

Article

Mitochondrial biogenesis in developing astrocytes regulates astrocyte maturation and synapse formation

Tamara Zehnder,[1,9] Francesco Petrelli,[1,9] Jennifer Romanos,[2,9] Eva C. De Oliveira Figueiredo,[1] Tommy L. Lewis, Jr.,[3,4,8] Nicole Déglon,[5,6] Franck Polleux,[3,4] Mirko Santello,[2,*] and Paola Bezzi[1,7,10,*]

[1]Department of Fundamental Neurosciences, Faculty of Biology and Medicine, University of Lausanne, Rue du Bugnon 9, 1005 Lausanne, Switzerland

[2]Institute of Pharmacology and Toxicology, University of Zurich, 8057 Zurich, Switzerland

[3]Department of Neuroscience, Columbia University, New York, NY 10032, USA

[4]Mortimer B. Zuckerman Mind Brain Behavior Institute, Columbia University, New York, NY 10032, USA

[5]Department of Clinical Neurosciences, Laboratory of Neurotherapies and Neuromodulation (LNTM), Lausanne University Hospital (CHUV) and University of Lausanne, 1011 Lausanne, Switzerland

[6]Neurosciences Research Center (CRN), Laboratory of Neurotherapies and Neuromodulation (LNTM), Lausanne University Hospital and University of Lausanne, 1011 Lausanne, Switzerland

[7]Department of Physiology and Pharmacology, Sapienza University of Rome, 00185 Rome, Italy

[8]Present address: Aging & Metabolism Program, Oklahoma Medical Research Foundation, Oklahoma City, OK 73104, USA

[9]These authors contributed equally

[10]Lead contact

*Correspondence: mirko.santello@pharma.uzh.ch (M.S.), paola.bezzi@unil.ch (P.B.)

https://doi.org/10.1016/j.celrep.2021.108952

SUMMARY

The mechanisms controlling the post-natal maturation of astrocytes play a crucial role in ensuring correct synaptogenesis. We show that mitochondrial biogenesis in developing astrocytes is necessary for coordinating post-natal astrocyte maturation and synaptogenesis. The astrocytic mitochondrial biogenesis depends on the transient upregulation of metabolic regulator peroxisome proliferator-activated receptor gamma (PPARγ) co-activator 1α (PGC-1α), which is controlled by metabotropic glutamate receptor 5 (mGluR5). At tissue level, the loss or downregulation of astrocytic PGC-1α sustains astrocyte proliferation, dampens astrocyte morphogenesis, and impairs the formation and function of neighboring synapses, whereas its genetic re-expression is sufficient to restore the mitochondria compartment and correct astroglial and synaptic defects. Our findings show that the developmental enhancement of mitochondrial biogenesis in astrocytes is a critical mechanism controlling astrocyte maturation and supporting synaptogenesis, thus suggesting that astrocytic mitochondria may be a therapeutic target in the case of neurodevelopmental and psychiatric disorders characterized by impaired synaptogenesis.

INTRODUCTION

The main period of synaptogenesis in the developing rodent cortex occurs during the second and third post-natal weeks, when astrocytes stop replicating and enter a phase of post-natal maturation in which they become capable of functionally interacting with synapses (Freeman, 2010). The temporal relationship between synapse and astrocyte maturation suggests that bi-directional interactions orchestrate the post-natal maturation of both in order to fine-tune the maturation of functional circuits (Allen and Eroglu, 2017; Petrelli and Bezzi, 2018).

It has long been speculated that neuronal activity plays an important role in regulating post-natal astrocyte maturation, and recent studies have shown that it regulates the astrocytic transcriptome and may therefore shape astrocyte/neuron metabolic cooperation (Hasel et al., 2017); in particular, glutamatergic neuronal activity can directly regulate post-natal astrocyte arborization (Morel et al., 2014). The genes that are developmentally regulated in immature astrocytes include those controlling glutamatergic signaling: the *GRM5* gene, which encodes metabotropic glutamate receptor 5 (mGluR5), is highly expressed in developing astrocytes during the first post-natal week, but its expression dramatically decreases by the third week (Cahoy et al., 2008; Zhang et al., 2016), and mGluR5 calcium (Ca^{2+}) signaling is particularly conspicuous in the soma and main processes of developing astrocytes (Buscemi et al., 2017; Sun et al., 2013). In line with its high level of expression in immature astrocytes, mGluR5 plays a crucial role in regulating the post-natal astrocyte growth and arborization (Morel et al., 2014), but the underlying cellular and molecular

mechanisms controlling mGluR5-dependent astrocyte morphogenesis are unknown.

Post-natal astrocyte maturation involves a complex series of events whose regulation is still not fully understood but occurs during the first 3 post-natal weeks (Bandeira et al., 2009; Ge et al., 2012), when astrocytes begin proliferating before undergoing the dramatic structural, molecular, and functional changes that enable them to reach maturity (Cahoy et al., 2008; Zhang et al., 2016; Stogsdill et al., 2017; Farhy-Tselnicker et al., 2017; Boisvert et al., 2018). These extensive changes in astrocyte proliferative activity and growth may impose energy constraints and distinct metabolic demands, as has recently been described in developing neurons (Beckervordersandforth et al., 2017; Zheng et al., 2016; Knobloch et al., 2013). The fact that mGluR5 signaling triggers post-natal astrocyte arborization (Morel et al., 2014) suggests that mGluR5 signaling may also drive distinct metabolic demands in order to accomplish the large number of fine processes typically seen in adult mammalian astroglia. It is known that energy metabolism requires rapid organization in order to respond to the changing status of cellular activities, and that any disturbance of this metabolic plasticity is related to impaired cell proliferation, differentiation, and maturation. However, whether and how a specific metabolic pathway is necessary to coordinate the development of astrocytes has never been investigated. A recent whole-cell transcriptome analysis of astrocytes has revealed the transient upregulation of many mitochondrial (mito) pathways during post-natal development (Boisvert et al., 2018), and this is supported by findings showing that the activation of mito biogenesis and the consequent metabolic shift toward oxidative phosphorylation (OxPhos) are crucial for the differentiation of glioblastoma cells into astrocytes (Xing et al., 2017). Activation of the mito biogenesis program (i.e., the growth and division of pre-existing mito) and the consequent increase in mito mass and activity are crucial cellular mechanisms that orchestrate the differentiation and maturation of many cell types, including neurons (Vayssière et al., 1992; Li et al., 2004; Cheng et al., 2012), and it has been shown that peroxisome proliferator-activated receptor gamma co-activator 1α (PGC-1α) is a master regulator of mito biogenesis (Wu et al., 1999).

Given the strategic peri-synaptic position of astrocytes, the aim of this study was to evaluate the importance of PGC-1α and mito biogenesis in the post-natal maturation of astrocytes and its impact on the formation and function of neighboring synapses. We used the conditional deletion of PGC-1α in immature astrocytes to establish the requirements for the PGC-1α regulation of astrocyte replication, outgrowth, and arborization during cortical development and the formation of synapses.

Our findings show that astrocytes mainly rely on a PGC-1α-dependent network of mito to stop their post-natal replication and reach maturity, and that a dysfunctioning mito network impairs correct post-natal astrocyte maturation and synaptogenesis, thus affecting post-natal cortical development. They also show that mGluR5 signaling regulates PGC-1α in developing astrocytes and therefore controls mito biogenesis and the post-natal development of astrocytes and their associated synapses.

RESULTS

Mitochondria in developing astrocytes show high OxPhos activity and ATP output

Increased levels of mRNA for genes encoding the proteins involved in the ETC (electron transport chain) and OxPhos are considered genetic correlates of greater OxPhos activity (Zheng et al., 2016; Agostini et al., 2016; Pooya et al., 2014; LeBleu et al., 2014). In order to obtain information about mito and glycolytic activities during astrocyte post-natal development *in vivo*, we purified astrocytes during the first 3 post-natal weeks (on post-natal day [P] 3, P14, and P20) and adulthood (on P50) (Figure 1A) using hGFAP-ECFP mice in which astrocytes express enhanced cyan fluorescent protein (ECFP) under the human glial fibrillary acidic protein (hGFAP) promoter (Hirrlinger et al., 2005), and analyzed the levels of mRNA encoding the key proteins regulating mito biogenesis (*PGC1*α, *PGC1*β, and *Esrra*) (Medeiros, 2008), OxPhos activity (*Cox5b*, *Cox41l*, *Atp5a1*, and *Cycs*) (Hackenbrock, 1968), and glycolysis (*AldoA*, *LDHA*) (Zheng et al., 2016), and the proteins regulating proliferation Ki67 (*MKI67*) (Ge et al., 2012) or associated with astrocyte maturation (Zhang et al., 2016; Boisvert et al., 2018), such as the glutamate transporter GLT1 (*SLC1A2*), connexin 30 and 43 (Cx30 and Cx43; *GJB6* and *GJA1*), and the inwardly rectifying potassium channel Kir4.1 (*KCNJ10*) (Figures 1B–1D, S1A, and S1B).

In line with the progressive maturation of astrocytes during the first 3 post-natal weeks (Hasel et al., 2017; Ge et al., 2012), RT-PCR analysis of the purified astrocytes (sorting yield >99% pure positive cells) (Figure S1C) revealed a decrease in proliferation (*MKI67*) (Figure S1A) and an increase in the levels of genes associated with astrocyte maturation (Figure S1B). The mRNA levels for genes encoding key proteins in mito biogenesis and OxPhos and glycolysis also increased during post-natal development and peaked during the third post-natal week (Figures 1B–1D), thus suggesting that OxPhos and glycolysis might be responsible for energy-providing metabolic circuits in developing astrocytes. The importance of OxPhos in developing astrocytes became clear when we analyzed astrocytes purified on P50 and found an unexpected decrease in the markers of OxPhos in comparison with astrocytes isolated during the second and third post-natal week. On P50, the upregulation of astrocyte markers GLT1, Cx30/43, and Kir4.1 and key proteins regulating glycolysis (Figures 1D and S1B) was paralleled by the downregulation of a number of genes regulating mito biogenesis and OxPhos activity (Scarpulla, 2011; Lin et al., 2005; Lelliott et al., 2006; Figures 1B and 1C), such as *PGC1*α ($-$86.49%), *PGC1*β ($-$82.34%), and *Esrra* ($-$78.14%) (Figure 1B) and the *ATP5a1* gene encoding for a crucial subunit of the mito ATP synthase ($-$53.98%) (Figure 1C). Interestingly, the decrease of *PGC1*α did not affect glycolysis, and the lactate levels in adult astrocytes were higher than those in immature astrocytes (Figures 1D and 1H). These findings suggested that a transient transition toward mito oxidative metabolism occurs in astrocytes during their post-natal maturation.

In order to explore the physiological relevance of the increased OxPhos and mito content in developing astrocytes, we also measured total cellular ATP levels and used a Seahorse XF analyzer to measure real-time oxygen consumption (OCR) in freshly isolated ECFP-positive astrocytes obtained on P14,

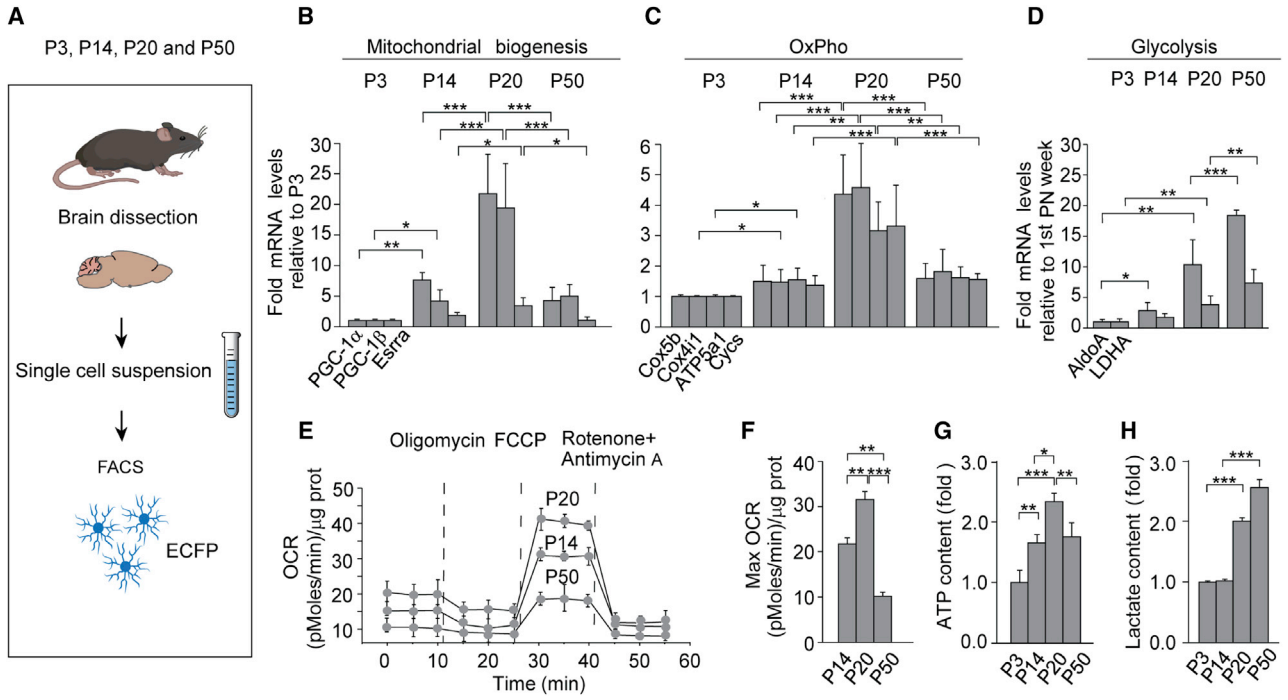

Figure 1. Developing astrocytes show increased transcription of mitochondrial genes and OCR associated with PGC-1α expression

(A) Illustration of fluorescence-activated cell sorting (FACS) sorting procedure.

(B–D) mRNA levels of FACS-sorted, ECFP-positive astrocytes. *p < 0.05, **p < 0.01; ***p < 0.001 (n = 6–10 mice in each group; one-way ANOVA followed by Bonferroni's post hoc correction).

(E) Real-time OCR of P14, P20, and P50 astrocytes as measured using a Seahorse XF analyzer.

(F) Indices of maximal mito respiratory as calculated from the OCR profiles. **p < 0.01, ***p < 0.001.

(G) ATP content in FACS-sorted, ECFP-positive astrocytes. *p < 0.05, **p < 0.01; ***p < 0.001 (n = 3–5 mice each group; one-way ANOVA followed by Bonferroni's post hoc correction).

(H) Lactate content in FACS-sorted, ECFP-positive astrocytes. ***p < 0.001 (n = 3–4 mice each group; one-way ANOVA followed by Bonferroni's post hoc correction).

All error bars represent mean values ± SEM of the three replicates at each time point.

P20, and P50. As expected, in comparison with the cells isolated on P50, those isolated on P20 had significantly more ATP content, higher basal and maximal OCR values (Figures 1E–1G), and less lactate content (Figure 1H).

Interestingly, these metabolic phenotypes were also observed in cultured astrocytes from day 5 *in vitro* (DIV5) to DIV20 (Figures S1F–S1K), when the cytoplasmic accumulation of elongated and hyperfused mito was particularly evident (Figures 2H and 2I). A series of biochemical analyses confirmed that mito biogenesis and OxPhos transcripts were all significantly upregulated (Figures S1D and S1E), and accordingly, OCR (but not ATP production) was significantly higher (Figures S1F and S1H), whereas that of ECAR and lactate were much lower (Figures S1G and S1I) on DIV5 than on DIV20.

Developing astrocytes show significantly greater cytosolic occupancy by the mito network than replicating and mature astrocytes

To determine whether increased expression of genes associated with mito biogenesis and OxPhos in developing astrocytes correlates with increased mito occupancy, we visualized the organelles in astrocytes *in vivo* with *in utero* electroporation (IUE) and permanently labeled single-cortical astrocytes with a plasmid expressing two transposable transgenes capable of genomic integration under the action of the piggyBac (PB) transposase, a cytoplasmic fluorescent protein (mTAGBFP2, pseudo-colored in gray), and a mito matrix-targeted fluorescent protein (mt-YFP, pseudo-colored in cyan) (Lewis et al., 2018). When electroporated on embryonic day (E) 15.5, this construct allowed us to analyze mito at high resolution in optically isolated, developing, or mature astrocytes on P10, P17, and P50 (Figures 2A–2C and S2B). We recognized the astrocytic identity of the electroporated cells by the expression of S100 calcium-binding protein β (S100β) (Buscemi et al., 2017; Richetin et al., 2020; Raponi et al., 2007; Figure S2A).

Morphometric analysis of mito occupancy in astrocytes revealed striking quantitative differences among P10, P17, and P50 (Figures 2D and S2B–S2D): at P17, mito formed a long, tubular, and interconnected network that occupied the majority of the soma (about 95%) and the proximal-to-distal portions of the main processes (about 90%) (on average 93.21%) (Figures 2E and 2F), whereas on P10 and P50, they formed a heterogeneous network of filamentous and fragmented mito that occupied only an average of 33.41% and 51.29%, respectively, of the soma and main processes (Figures 2E, 2F, and S2B–S2D).

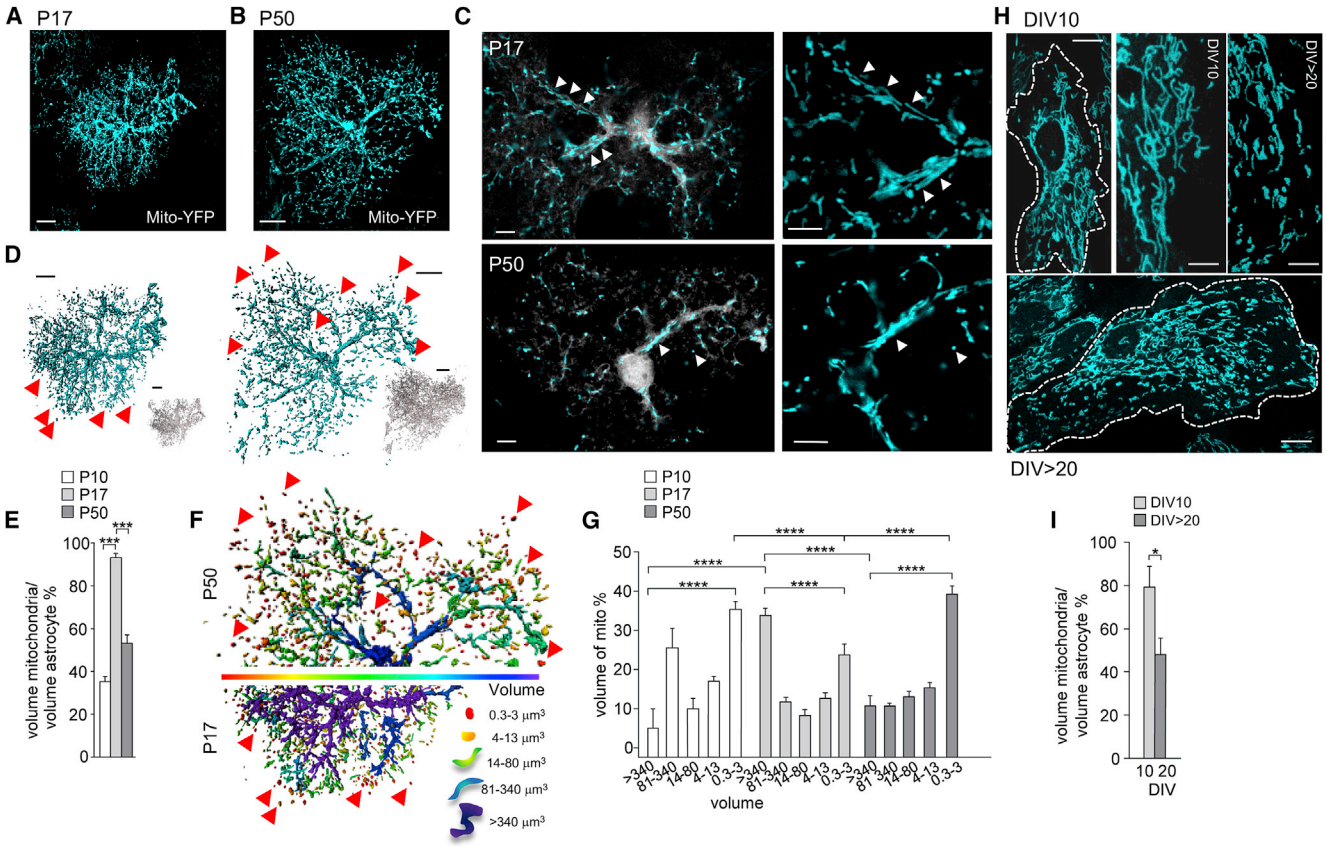

Figure 2. Cytosolic occupancy and distribution of mitochondria during post-natal development

(A and B) Confocal sections of mito visualized with IUE of mitoYFP and mTAGBFP2 cytoplasmic filler. Scale bars: 10 μm.

(C) Single confocal planes of the images in (A) and (B). Arrowheads indicate the mito network in the main processes of astrocytes on P17 and P50. Scale bars: 5 μm.

(D) Rendering of the two reconstructed astrocytes and mito network shown in (A) and (B). Arrowheads indicate some of the fragmented mito (0.3–3 μm^3) highlighted in (F).

(E) Quantification of the percentage of P10, P17, and P50 astrocytes occupied by mito. ***$p < 0.001$ (n = 4–5 mice each group; unpaired Student's t test).

(F) Pseudocolor-coded representation of volume/sphericity of the two reconstructed mito networks shown in (A) and (B).

(G) Quantification of the distribution of mito morphology (n = 5–6 mice each group; one-way ANOVA followed by Bonferroni's post hoc correction; ****$p < 0.0001$).

(H) Confocal sections of mito in cultured astrocytes on DIV10 and DIV > 20 visualized with MitoTracker (cyan). The dotted lines show the astrocyte boundaries. Scale bars: 20 μm and 5 μm for high magnifications.

(I) Quantification of the volume of cultured astrocytes occupied by mito on DIV10 and DIV > 20 (n = 3 mice, 7–10 cells in each group; unpaired Student's t test, *$p < 0.05$).

All error bars represent mean values ± SEM.

The increase in mito occupancy between P10 and P17 was mainly due to an increase in mito volume (643.72 ± 32.48 and 1,871.21 ± 128.75 μm^3 at P10 and P17, respectively), whereas the decrease in mito occupancy between P17 and P50 was mainly due to an increase in astrocyte volume (2,003.65 ± 130.88 and 3,573.54 ± 255.09 μm^3 at P17 and P50, respectively) rather than a decrease in mito volume (1,871.21 ± 128.75 and 1,926.25 ± 235.65 μm^3 at P17 and P50, respectively). The differences in mito occupancy among P10, P17, and P50 became apparent when sub-dividing mito on the basis of their volume: the contribution of highly interconnected mito (i.e., those with a volume > 340 μm^3) to total volume was significantly smaller on P10 and P50 than on P17, whereas the contribution of fragmented mito (i.e., those with a volume of 0.3–13 μm^3) was significantly greater on P10 and P50 than on P17 (Figures 2F, 2G, and S2B).

To confirm the validity of this observation *in vitro*, we isolated and cultured pure astrocytes from post-natal mouse pups and visualized their mito using a MitoTracker at DIV10 and DIV25 while examining mRNA levels for genes regulating astrocytic proliferation and maturation (Figures S1J and S1K). In line with the progressive maturation of astrocytes, the downregulation of the *MKI67* and *TOP2A* genes regulating proliferation was paralleled by the upregulation of genes encoding GLT1, CX30/43, and Kir4.1 (Figures S1J and S1K). Interestingly, quantitative measurement of mito occupancy in developing and mature astrocytes showed that they were highly conserved *in vitro* (Figures 2H and 2I): mito in developing astrocytes occupied 79.2% of cell

volume, whereas the mito in mature cells occupied 48.4% (Figure 2I). We therefore concluded that mito occupancy is different in developing and mature cortical astrocytes *in vivo* and *in vitro*.

PGC-1α controls mito content in developing astrocytes

Because PGC-1α is a master regulator of mito biogenesis and function, its deletion induces a significant decrease in mito mass and consequently a significant decrease in OxPhos machinery and mito activity (Li et al., 2004; Cheng et al.,2012; LeBleu et al., 2014; Jiang et al., 2016; Leone et al., 2005; Tran et al., 2016). We therefore used the conditional PGC-1α knockout mice as a model to determine the role of mito biogenesis in developing astrocytes *in vitro* and *in vivo* (Figure S4A). For the *in vitro* experiments, astrocytes isolated from the newborn pups of hGFAPCre^{ERT2}PGC1α$^{loxp/loxp}$;R26-tdTomato$^{loxp/loxp}$ and control hGFAP:Cre^{ERT2}R26-tdTomato$^{loxp/loxp}$ mice were treated with tamoxifen (TAM) for DIV7. The immunostaining of cultured cells revealed a specific recombination in cultured astrocytes (48%; Figures S3E and S3F), and the RT-PCR analysis a significant downregulation of the genes associated with mito biogenesis (Figure 3H) and OxPhos activity (Figure S3G).

For experiments *in vivo*, the conditional knockout mice were created by treating mice with TAM for 8 days starting on P5 (respectively referred to as aPGC1αcKO-tdTomato and hGFAP-tdTomato mice). Confocal analysis of cortical tissue revealed specific recombination in astrocytes (>95% of tdTomato expressed glutamine synthase; recombination of 52.25% [L1], 59% [L2/3], 58.7% [L5]; Figures S3A, S3C, S4A, and S4E), with no recombination in cortical neurons (0% of tdTomato expressed NeuN; Figure S3B), and RT-PCR analysis confirmed a significant reduction of PGC-1α mRNA levels (−44%) (Figure S3D).

Morphological analysis of the mito in the recombined cells carrying the deletion of PGC-1α revealed a significant change in mito morphology (i.e., many more punctated mito) and a significant reduction in cytosolic occupancy (−61.56% and −48.53% *in vitro* and *in vivo*, respectively) in comparison with the controls (Figures 3A–3E and 3G). The effect of PGC-1α deletion on mito was accompanied by a significant decrease in basal and maximal OCR (Figure S3I) or ATP content (Figure S3J), and with a significant increase in basal glycolysis (Figure 3K) and lactate content (Figure 3L). Interestingly, such metabolic changes were not significant after normalization to mito volume (Figures 3I and 3J), thus supporting the hypothesis that the deletion of PGC-1α in developing astrocytes decreases mito content without affecting mito function. Finally, mito occupancy and metabolic changes were all rescued when *PGC-1α* was re-expressed on DIV3 by means of an astrocyte-specific lentiviral vector (LentiPGC1α) (Petrelli et al., 2020; Colin et al., 2009; Pannasch et al., 2014; Figures 3F, 3G, 3M–3Q, and S3H), thus suggesting that PGC-1α promotes mito biogenesis and a coordinated shift toward mito activity in developing astrocytes.

Conditional deletion of PGC-1α from developing astrocytes compromises post-natal proliferation and maturation of astrocytes

A number of studies have shown that mito plays a critical role in the regulation of proliferation, differentiation, and maturation processes (Diebold et al., 2019; Yao et al., 2019; Zheng et al., 2018; Khacho et al., 2019; Gotoh et al., 2018). We therefore checked the effects of decreased mito occupancy in the cortical development of aPGC1αcKO-tdTomato mice (Figure S4A). The overall brain morphology of aPGC1acKO mice did not show any gross anatomical differences, overt alterations in laminar organization (Figures 4A, S4B, and S4C), or any sign of apoptosis (Figure S4D), but DAPI staining revealed a significant increase in cell frequency (+9.01% for L2,3 and +9.2% for L5, corresponding to +338.69 ± 98.5 DAPI and +345.49 ± 130.5 DAPI for L2,3 and L5, respectively) (Figure 4B). We further evaluated the change in tdTomato astroglial and neuronal density and in line with the DAPI staining, there was an increase in the frequency of tdTomato astrocytes (+118.11% and +97.6% for L2,3 and L5, corresponding to +176.74 ± 40.3 and +186.3 ± 44.5 in L2,3 and L5, respectively), but not in the frequency of CTIP2-labeled neurons (Figures 4C and S4B). The number of DAPI nuclei was about three times higher than the number of recombined tdTomato astrocytes; thus, in order to check which cell type(s) could account for the increased number of DAPI nuclei, we started by analyzing non-recombined astrocytes (i.e., GS$^+$ and tdTomato$^-$ cells) and found a significant increase in both L2,3 and L5 (+11.839% and +12.923% for L2,3 and L5; Figure S4E), respectively, corresponding to +82.5 ± 30.6 and +110.34 ± 22.5 GS$^+$ cells. Subsequently, we also investigated whether neuron-glia antigen 2 (NG2) glia could account for the increased number of DAPI-stained cells. Indeed, among other glial cells, the NG2 progenitors of oligodendrocytes (Levine et al., 2001) represent the fourth major glial population in the cortex (Dawson et al., 2000, 2003; Nishiyama et al., 2002; Peters, 2004) and may be affected by the hGFAP promoter (Weng et al., 2019). Immunostaining of NG2 showed no co-localization with tdTomato$^+$ cells (Figures S4F–S4I) but a significant increase in the number of NG2$^+$ cells (+30.04% in L2,3 and +35.66% in L5) corresponding to +77.15 ± 12.5 and +81.34 ± 9.6 (Figure S4J). These findings indicated that the deletion of PGC-1α in a subset of astrocytes affects the proliferation of neighboring glial cells.

Given the well-established role of PGC-1α in cell proliferation, we investigated whether this cortical abnormality was due to changes in post-natal cell proliferation. The long-term BrdU pulse-chase experiments revealed that BrdU staining was significantly increased in both recombined (tdTomato$^+$ astrocytes; +40.58% for L2,3 and +102.95% for L5) and non-recombined astrocytes (GS$^+$/tdTomato$^-$ astrocytes; +39.13% for L2,3 and +62.69% for L5) (Figures 4D, 4E, S4K, and S4L), as well as in NG2$^+$ cells (+36.31% for L2,3 and +31.25% for L5) (Figures S4M and S4N), thus confirming the increased proliferation of astrocytes and NG2 cells in the cortical tissue of aPGC1αcKO mice.

Because the complex functions of mature astrocytes depend on their elaborate structure (Stogsdill et al., 2017; Sakers and Eroglu, 2019), we investigated the effects of *PGC1α* deletion on morphogenesis of astrocytes. Morphometric analysis of their elaborate structure revealed a dramatic morphological phenotype: the *PGC1α*-deleted tdTomato astrocytes had smaller domains (−19% in diameter in L2/3 and −21.9% in L5) (Figures 4F–4H), fewer branches (−34.3%, 20 μm from the soma; Figures 4K–4M), and clearly less distance between somas (−53%; Figures

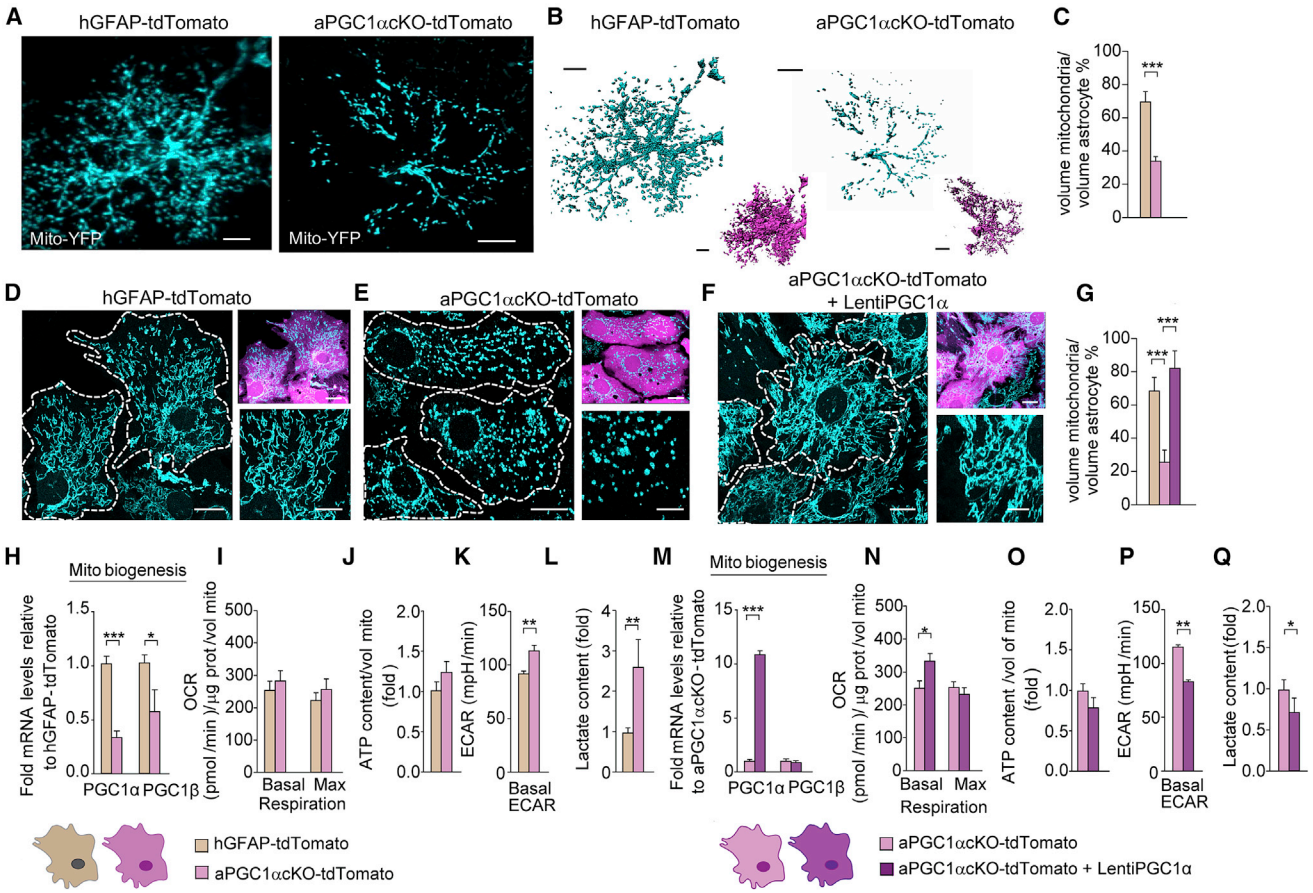

Figure 3. PGC-1α controls mitochondrial biogenesis in developing astrocytes

(A) Confocal sections of mito in L5 cortical astrocytes on P17 visualized with IUE of mitoYFP and mTAGBFP2 cytoplasmic filler. Scale bar: 10 μm.

(B) Rendering of the two reconstructed astrocytes and mito networks shown in Figure 3A. Scale bar: 7 μm.

(C) Quantification of the percentage of astrocytes volume occupied by mito. ***$p < 0.001$ (n = 3 mice each group; unpaired Student's t test).

(D–F) Confocal sections of mito in cultured astrocytes as visualized with MitoTracker (mitochondria = cyan, tdTomato$^+$ astrocytes = magenta). Dotted lines show astrocyte boundaries. Scale bars: 20 μm and 5 μm for high-magnification images.

(G) Quantification of volume occupied by mito in cultured astrocytes. ***$p < 0.001$ (n = 3 mice in each group; one-way ANOVA followed by Bonferroni's post hoc correction).

(H) mRNA levels of PGC1α and PGC1β in cultured astrocytes. *$p < 0.05$; ***$p < 0.001$ (n = 4–6 biologically independent samples; unpaired Student's t test).

(I) Indices of mito respiratory function calculated from the OCR profile of cultured astrocytes measured on DIV10 (n = 5 biologically independent samples; unpaired Student's t test).

(J) ATP content in cultured astrocytes measured on DIV10 (n = 5 biologically independent samples; unpaired Student's t test).

(K) Indices of glycolytic pathway activation in cultured astrocytes on DIV10. **$p < 0.01$ (n = 5 biologically independent samples; unpaired Student's t test).

(L) Lactate content in cultured astrocytes on DIV10. **$p < 0.01$ (n = 5 biologically independent samples; unpaired Student's t test).

(M) mRNA levels of PGC1α and PGC1β in cultured astrocytes. ***$p < 0.001$ (n = 3 biologically independent samples; unpaired Student's t test).

(N) Indices of mito respiratory function as calculated from the OCR profile of cultured astrocytes measured on DIV10. *$p < 0.05$ (n = 5 biologically independent samples; unpaired Student's t test).

(O) ATP content in cultured astrocytes measured on DIV10 (n = 5 biologically independent samples; unpaired Student's t test).

(P) Indices of glycolytic pathway activation calculated in cultured astrocytes. **$p < 0.01$ (n = 5 biologically independent samples; unpaired Student's t test).

(Q) Lactate content in cultured astrocytes on DIV10. *$p < 0.05$ (n = 3 biologically independent samples; unpaired Student's t test).

All error bars represent the mean values ± SEM of three replicates at each time point.

4I and 4J), thus suggesting a possible overlapping domain that is typical of immature astrocytes on P7–P10 (Stogsdill et al., 2017). Similar results were found in non-recombined astrocytes (−18.7% in the diameter, −29.5% in the number of branches 20 μm from the soma, n = 3 mice, $p < 0.05$, unpaired Student's t test). Overall, these observations indicated that PGC1α regulates post-natal proliferation and maturation of astrocytes.

mGluR5 controls PGC-1α levels and mito biogenesis in developing astrocytes

Mito content and function are finely tuned to satisfy cell-specific metabolic and signaling demands (Hock and Kralli, 2009) and are controlled by a highly interconnected network of transcription factors, such as mammalian target of rapamycin (mTOR) (Morita et al., 2013), a master regulator of a broad set of nuclear genes,

CellPress
OPEN ACCESS

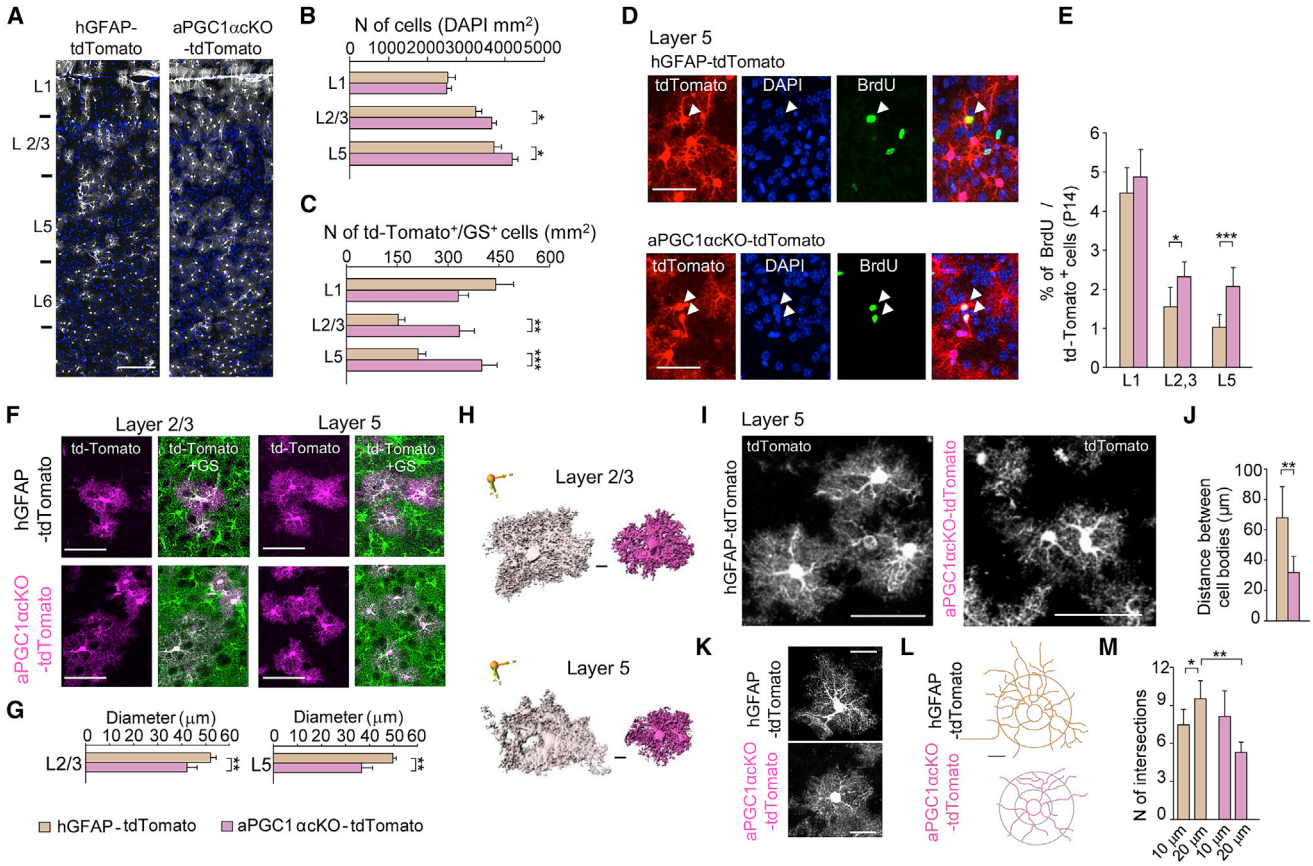

Figure 4. Selective and inducible deletion of astrocyte PGC-1α impairs the maturation of cortical astrocytes

(A) Confocal sections of tdTomato astrocytes (gray) and DAPI staining (blue) in prefrontal cortex (PFC) on P40. Scale bar: 100 μm.

(B) Quantification of DAPI-stained cells per mm^2 in PFC on P40. *p < 0.05 (n = 3 mice in each group; unpaired Student's t test).

(C) Quantification of td-Tomato$^+$ astrocytes in PFC on P40. **p < 0.01, ***p < 0.001 (n = 4 mice each group; unpaired Student's t test).

(D) Confocal sections of tdTomato$^+$ astrocytes (red), and immunostaining for BrdU (green) and DAPI (blue) in PFC on P14. Scale bar: 50 μm.

(E) Quantification of BrdU and tdTomato$^+$ cells in PFC on P14. *p < 0.05, ***p < 0.001 (unpaired Student's t test).

(F–H) Quantification of astrocyte complexity in PFC on P40.

(F) Confocal sections of tdTomato$^+$ astrocytes (magenta) and immunostaining for GS (green) in PFC on P40. Scale bar: 50 μm.

(G) Diameter of tdTomato$^+$/GS$^+$ astrocytes in PFC on P40. **p < 0.01 (n = 4 mice in each group; unpaired Student's t test).

(H) Representative 3D surface rendering of tdTomato$^+$ astrocytes on P40. Scale bar: 10 μm.

(I) Confocal sections show tdTomato$^+$ astrocytes in PFC sections on P40. Scale bar: 50 μm.

(J) Distance between cell bodies of tdTomato$^+$ astrocytes on P40. **p < 0.01 (n = 4 mice each group; unpaired Student's t test).

(K) High magnification of individual astrocytes. Scale bar: 20 μm.

(L and M) Sholl analysis of tdTomato$^+$ astrocytes in PFC on P40. Scale bar: 10 μm. *p < 0.05, **p < 0.01 (n = 3 mice in each group; unpaired Student's t test).

All error bars represent mean values ± SEM (4–6 brain slices in each mouse).

including *PGC-1α*. Developing astrocytes transiently express high levels of mGluR5 (Buscemi et al., 2017; Sun et al., 2013), and it is known that mGluR5 signaling induces mTOR activation (Hou and Klann, 2004; Volk et al., 2007). To determine whether mGluR5 signaling regulates mTOR and PGC-1α in developing astrocytes, we performed western blot analyses of cultured astrocytes (DIV15) coupled with pharmacological or genetic manipulations (Figure S5A). Our results confirmed that both the phospho-mTOR/mTOR ratio and PGC-1α were regulated in a calcium-dependent manner by mGluR5 signaling (Figures S5A–S5C).

Genetic ablation of *mGluR5* in astrocytes allowed us to analyze the role of mGluR5 signaling in controlling the astrocytic mito content *in vitro* and *in vivo*. We cross-bred mGluR5$^{loxp/loxp}$ (Barnes et al., 2015) mice with hGFAP:Cre^{ERT2} (Petrelli et al., 2020; Hirrlinger et al., 2006) and R26-tdTomato$^{loxp/loxp}$ (Morel et al., 2014) fluorescent reporter mice and induced the recombination *in vitro* and *in vivo* by treating the cells or the progeny inheriting both alleles with TAM for 8 days (from DIV3 or from P5, respectively). The TAM-treated mice with the mGluR5 deletion will hereinafter be referred to as amGluR5cKO-tdTomato mice. TAM-treated hGFAP:Cre^{ERT2}R26-tdTomato$^{loxp/loxp}$ cultured cells or mice were used as controls (i.e., hGFAP-tdTomato). We first checked the effect of astrocyte-specific *mGluR5* conditional deletion on mito morphology by visualizing mito *in vivo* with IUE and *in vitro* with MitoTracker on P17 and DIV15, when TAM treatment led a significant reduction in the mRNA levels of *mGluR5* and

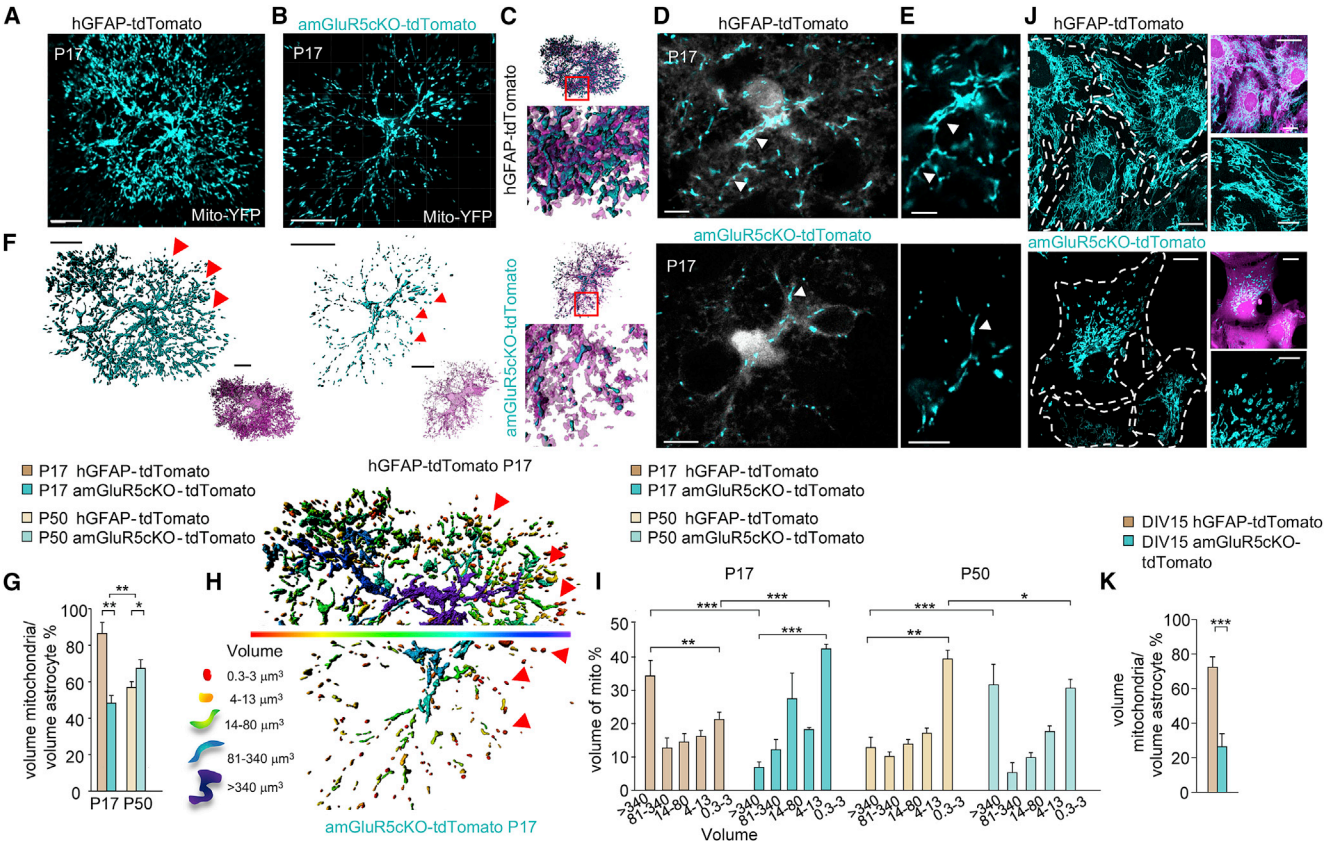

Figure 5. Mitochondrial content and distribution are disrupted in mGluR5-deficient astrocytes

(A and B) Confocal sections show mito in L5 cortical astrocytes on P17 visualized with IUE of mitoYFP and mTAGBFP2 cytoplasmic filler. Scale bar: 10 μm.

(C) Rendering of the two reconstructed astrocytes and mito networks shown in (A) and (B). Red boxed regions highlight the significant depletion of mito in small processes of amGluR5cKO astrocytes in comparison with control hGFAP-tdTomato astrocytes.

(D and E) Single confocal planes of the images shown in (A) and (B). Arrowheads indicate the network of mito in the main processes. Scale bar: 5 μm.

(F) Rendering of two reconstructed astrocytes and mito networks shown in (A) and (B). Arrowheads indicate some of the fragmented mito (0.3–3 μm^3) highlighted in (H).

(G) Quantification of mito occupancy of P17 and P50 tdTomato$^+$ astrocytes. *p < 0.05, **p < 0.01 (n = 3–4 mice in each group; unpaired Student's t test).

(H) Pseudocolor-coded representation of volume/sphericity of the two reconstructed mito networks shown in (A) and (B).

(I) Quantification of the distribution of mito morphology. *p < 0.05, **p < 0.01, ***p < 0.001 (n = 3–4 mice in each group; one-way ANOVA followed by Bonferroni's post hoc correction).

(J) Confocal sections of mito in cultured astrocytes as visualized with MitoTracker (mito = cyan, tdTomato$^+$ astrocytes = magenta). The dotted lines show astrocyte boundaries. Scale bar: 20 μm and 5 μm.

(K) Quantification of the volume of astrocytes occupied by mito on DIV10. ***p < 0.001 (n = 3 mice in each group; unpaired Student's t test).

All error bars represent mean values ± SEM.

PGC-1α (Figures S5E–S5G). Morphometric analysis revealed that mito morphology and occupancy were both dramatically different from those observed in controls *in vivo* (Figures 5A–5F) and *in vitro* (Figures 5J and 5K). Mito in mGluR5-deficient astrocytes were short (0.1–4.5 μm) and occupied only an average of about 45% of the soma and main processes (Figures 5G). The elongated interconnected network present in control developing astrocytes at P17 (Figures 5A and 5C–5E) was replaced by a significantly smaller and more heterogeneous mito network in mGluR5-deficient astrocytes (Figures 5B–5E), where the contribution of fragmented mito (i.e., those with 0.3–13 μm^3 of volume) over the total volume of the mito network was significantly increased compared with control (~2-fold; Figures 5H and 5I). Interestingly, the analysis of mito distribution and morphology on P50 showed a significant increase in mito occupancy and a morphology similar to that of the control astrocytes on P17 with an elongated interconnected network of mito (Figures 5G, 5I, and S5H), thus suggesting a slowing in the process of mito biogenesis in the absence of mGluR5.

We complemented these morphological observations by determining the extent to which mito activity was impaired in the absence of mGluR5. Metabolic measurements identified an approximately 50% reduction in basal and maximal OCR, a 30% reduction in ATP content, and a concomitant increase in the basal level of ECAR (25%) (Figure S5J). Interestingly, as previously shown in the absence of PGC-1α, when normalized to mito volume, there was no difference in OCR or ATP content between the amGluR5cKO and control mice (Figures S5I and S5K), thus supporting the hypothesis that the deletion of mGluR5 in

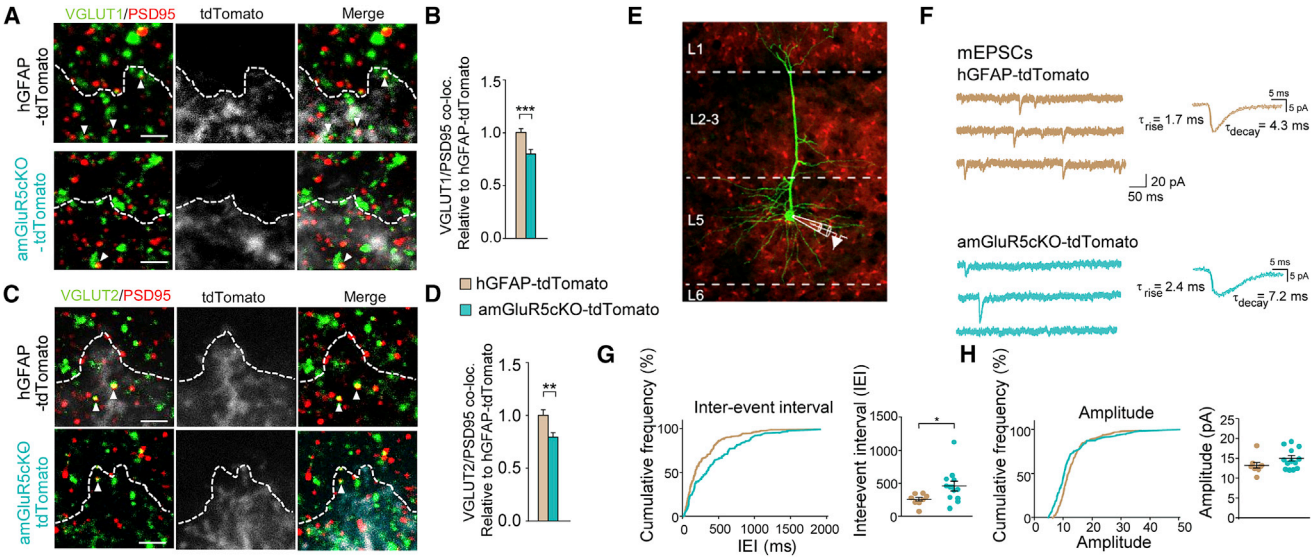

Figure 6. Astrocytic mGluR5 controls the number and function of excitatory synapses

(A and C) Confocal sections of intra-cortical (VGLUT1, green; PSD95, red) and thalamo-cortical excitatory synapses (VGLUT2, green; PSD95, red) inside the tdTomato astrocyte territory. Scale bar: 2 μm. Dotted lines show astrocyte boundaries, and arrowheads mark co-localized puncta.

(B and D) Quantification of intra-cortical (B) and thalamo-cortical (D) co-localized puncta in the tdTomato astrocyte territories in L5 of PFC on P40. $^{**}p < 0.01$, $^{***}p < 0.001$ (n = 3–4 mice in each group; unpaired Student's t test).

(E) Patch-clamp recording from the soma of a biocytin-labeled L5 pyramidal cell and tdTomato$^+$ astrocytes in the medial prefrontal cortex (mPFC) on P40.

(F) Representative traces of whole-cell mEPSC recordings. Average mEPSCs are shown below the traces.

(G) Cumulative frequency plots of inter-event intervals (IEIs) from the traces in (F) and comparison of average mEPSC IEIs in control mice (266.8 ± 31.6 ms, n = 8) and amGluR5cKO-tdTomato mice (468.6 ± 68.5 ms, n = 13).

(H) Cumulative frequency plot of mEPSC amplitude from the traces in (F) and comparison of average mEPSC amplitudes in control mice (13.3 ± 0.8 pA) and amGluR5cKO-tdTomato mice (15 ± 0.7 pA). The data points represent individual cells. $^{*}p < 0.05$ (unpaired Student's t test).

All error bars represent mean values ± SEM.

developing astrocytes decreases the content of mito without affecting mito functions.

Analysis of the proliferation and morphology of recombined and non-recombined astrocytes (i.e., tdTomato$^+$ and tdTomato$^-$/GS$^+$ cells, respectively) carrying the *mGluR5* deletion showed increased proliferative activity on P14 (Figures S5L and S5M) and, consistently, an increased number of astrocytes on P40 (Figures S5O, S5P, and S5W) without any further changes in the thickness of the cortical layers (Figures S5X and S5Y). Similar as for the deletion of PGC-1α, we also found a significant increase in the proliferative activity (Figure S5N) and the number of NG2$^+$ cells (Figure S5Q). Furthermore, single-cell analyses of astrocyte morphology showed that the diameter of the individual astrocytic territories, the distance between cell bodies, and the number of branching points were significantly decreased compared with control astrocytes (Figures S5R–S5V), thus confirming a recently reported delay in astrocytic arborization in the absence of mGluR5 (Morel et al., 2014). Our results demonstrated that mGluR5 signaling regulates *PGC-1α* and mito biogenesis and plays a critical role in the post-natal maturation of astrocytes.

Aberrant astrocyte maturation affects the number and function of excitatory synapses

Because astrocytes are key controllers of excitatory synaptogenesis (Allen and Eroglu, 2017), we investigated whether the dysfunction in post-natal astrocyte maturation induced by *PGC-1α* or *mGluR5* deletion impedes synaptogenesis. The synapses were labeled by means of apposition of the presynaptic markers vesicular glutamate transporters 1 and 2 (VGLUT1 and VGLUT2) and postsynaptic density protein 95 (PSD95) (Stogsdill et al., 2017). Strikingly, we found that synapse density within the territory of *PGC1α*- or *mGluR5*-deficient td-Tomato$^+$ astrocytes was significantly reduced compared with control hGFAP-tdTomato astrocytes (−25.5% for VGLUT1 and −29.6% for VGLUT2 in aPGC1αcKO-tdTomato; −20.3% for VGLUT1 and −20.5% for VGLUT2 in amGluR5cKO-tdTomato; Figures 6A–6D and S6A–S6D), thus confirming that impaired astrocyte morphogenesis affects the formation of excitatory synapses (Petrelli and Bezzi, 2018).

In order to evaluate the functional significance of these changes, we performed whole-cell patch-clamp recordings of miniature excitatory post-synaptic currents (mEPSCs) in L5 pyramidal neurons from the PFC of P40 amGluR5cKO-tdTomato and control mice (Figures 6E and 6F). This analysis confirmed a significant reduction in the number of detected synaptic events (inter-event interval, 266.8 ± 31.6 ms in the controls and 468.6 ± 68.5 ms in the amGluR5cKO mice) (Figures 6F and 6G) and a slowing in their kinetics (rise time: 2.1 ± 0.1 ms in the controls and 2.4 ± 0.1 ms in amGluR5cKO mice; decay time: 4.9 ± 0.3 versus 6.2 ± 0.3 ms) (Figures S6E and S6F), without any significant effect on their amplitude (Figures 6F and 6H). In the voltage-clamp recordings, we found no

significant difference in the capacitance, access resistance, and input resistance of neurons for both genotypes (capacitance: control 139.5 ± 28 pF, n = 8 cells, amGlu5cKO 139 ± 24 pF, n = 13 cells; access resistance: control 10.9 ± 3.2 MΩ, n = 8 cells, amGlu5cKO 12.5 ± 1.5 MΩ, n = 13 cells; input resistance: 87.4 ± 19.4 MΩ, n = 8 cells), amGlu5cKO (89.6 ± 33 MΩ, n = 13 cells, $p > 0.05$). These results also suggest that mGluR5 deletion in astrocytes may regulate synaptic maturation. Hence, in other areas of the CNS, more immature synapses have been shown to exhibit lower probability of release and slower synaptic events (Wall et al., 2002; Taschenberger and von Gersdorff, 2000; Cathala et al., 2005) in analogy with those detected in the mPFC of mice carrying astrocyte-specific mGluR5 deletion. Yet, we cannot exclude that other mechanisms may also be responsible for these alterations.

Re-expression of PGC-1α in mGluR5-deficient astrocytes restores astrocyte morphogenesis and synaptogenesis

The prominent role of astrocytic PGC-1α in regulating post-natal astrocyte development and synapse formation was confirmed *in vivo* by re-expressing PGC-1α in developing astrocytes on P5. The amGluR5cKO and control tdTomato mice were injected with an astrocyte-specific Lentivirus expressing PGC-1α or GFP or DsRed (Figures S7A and S7B; Petrelli et al., 2020; Humbel et al., 2021). RT-PCR analysis showed that the injection of Lenti:PGC-1α into the PFC of amGluR5cKO-tdTomato mice significantly increased *PGC1α* mRNA levels (Figure S7C). The morphometric analysis of mito showed that the decrease in mito occupancy and distribution in the absence of mGluR5 was rescued by LentiPGC-1α (Figures 7A–7G), thus demonstrating that the effect of mGluR5 deletion on mito maturation in astrocytes requires PGC-1α. Consistent with the effects on the mito network in astrocytes, subsequent analysis showed that LentiPGC-1α restored the proliferative capacity and the number of recombined and non-recombined astrocytes (Figures S7F and S7G). Astrocyte morphology showed that recombined td-Tomato$^+$ astrocytes in the mice injected with LentiPGC1α had a radius, volume, and distance between soma comparable with control astrocytes (Figures 7H–7L), thus indicating that the re-expression of PGC-1α restored the correct morphogenesis of astrocytes. Finally, and in line with the rescue obtained in developing astrocytes, confocal analysis showed significantly more excitatory synapses in the domains of mGluR5-deficient astrocytes of the infected mice (Figures 7M, 7N, S7H, and S7I), thus confirming that the correct expression of PGC-1α in developing astrocytes is crucial for post-natal synaptogenesis.

Taken together, our data show that mGluR5 signaling is required for the correct formation and function of cortical excitatory synapses through regulation of PGC-1α in developing astrocytes.

DISCUSSION

The findings of this study reveal a mechanism linking mito biogenesis in developing astrocytes to cortical synaptogenesis. Our results unravel the crucial role of astrocytic mito in regulating post-natal astrocyte proliferation and maturation, and support the formation and function of the associated synapses.

The cellular and molecular mechanisms regulating cell metabolism in mature astrocytes have been extensively investigated over the years (Magistretti and Allaman, 2018; Bouzier-Sore and Pellerin, 2013; Calì et al., 2019), and there is a general consensus that, although neurons are highly oxidative, astrocytes are predominantly glycolytic, which means that they extract energy from glucose by producing lactate and pyruvate (Weber and Barros, 2015; Magistretti et al., 2015; Azzalin et al., 2020). Furthermore, and in line with the glycolytic nature of astrocytes, the presence of modest mito respiration in mature astrocytes has recently been confirmed *in vivo* (Supplie et al., 2017).

The importance of mito activity in astrocytes is still largely unknown, but the findings of recent studies indicate that mitos in mature astrocytes are crucially important for the maintenance of homeostatic functions and the associated synapses (Motori et al., 2013; Ignatenko et al., 2018; Göbel et al., 2020). Our results provide the evidence that mito occupancy varies widely during post-natal astrocyte development. As in cells with a high oxidative capacity (Puigserver and Spiegelman, 2003; Kamei et al., 2003), PGC-1α and PGC-1β are highly enriched in developing astrocytes (but not replicating astrocytes) *in vitro* and *in vivo*. In line with the identification of PGC-1α as a master regulator of mito biogenesis and respiratory function (Wu et al., 1999), the deletion of *PGC1α* in astrocytes leads to a significant decrease in mito content, the genes encoding for ETC components underlying OxPhos, and, consequently, mito respiration. Our study therefore provides evidence of a transient requirement of mito biogenesis and very probably OxPhos in developing astrocytes at a time associated with the termination of proliferation and the initiation of functional and morphological maturation (i.e., during the second and third post-natal weeks, and from DIV7 to DIV20), as previously shown in neuronal (Zheng et al., 2016; Agostini et al., 2016; Agathocleous et al., 2012; Homem et al., 2014; Khacho et al., 2016) and glioblastoma cells (Xing et al., 2017).

The genetic ablation of mito biogenesis by means of the deletion of *PGC1α* in astrocytes induces prolonged proliferation and inhibition of developmental morphogenesis of astrocytes. PGC-1α may play a general role in regulating circuit connectivity in the developing brain because low levels of PGC-1α inhibit not only the developmental growth of the astroglial domain (i.e., arborization and the branching of processes), but also neurite outgrowth and the dendritic arbors of developing neurons (Cheng et al., 2012; Lin et al., 2004).

PGC-1α and mito biogenesis are regulated by a number of signaling pathways and transcription factors (Finck and Kelly, 2006), including CREB (Herzig et al., 2001), cyclic AMP-dependent protein kinase (Zong et al., 2002), calcium/calmodulin-dependent kinase (Czubryt et al., 2003), and mTOR (Cunningham et al., 2007), a kinase that regulates cell growth, size, and survival (Kozorovitskiy et al., 2015). It is therefore likely that the signals that increase cyclic AMP and cytosolic calcium levels and the mTOR signaling cascade also increase PGC-1α expression and mito biogenesis. Interestingly, proliferating astrocytes express high levels of mGluR5 during the first 2 weeks of post-natal development (Buscemi et al., 2017; Sun et al., 2013; Cai et al., 2000), a time preceding peak *PGC1α* levels and OxPhos activity, and a number of studies have shown that the activation

CellPress
OPEN ACCESS

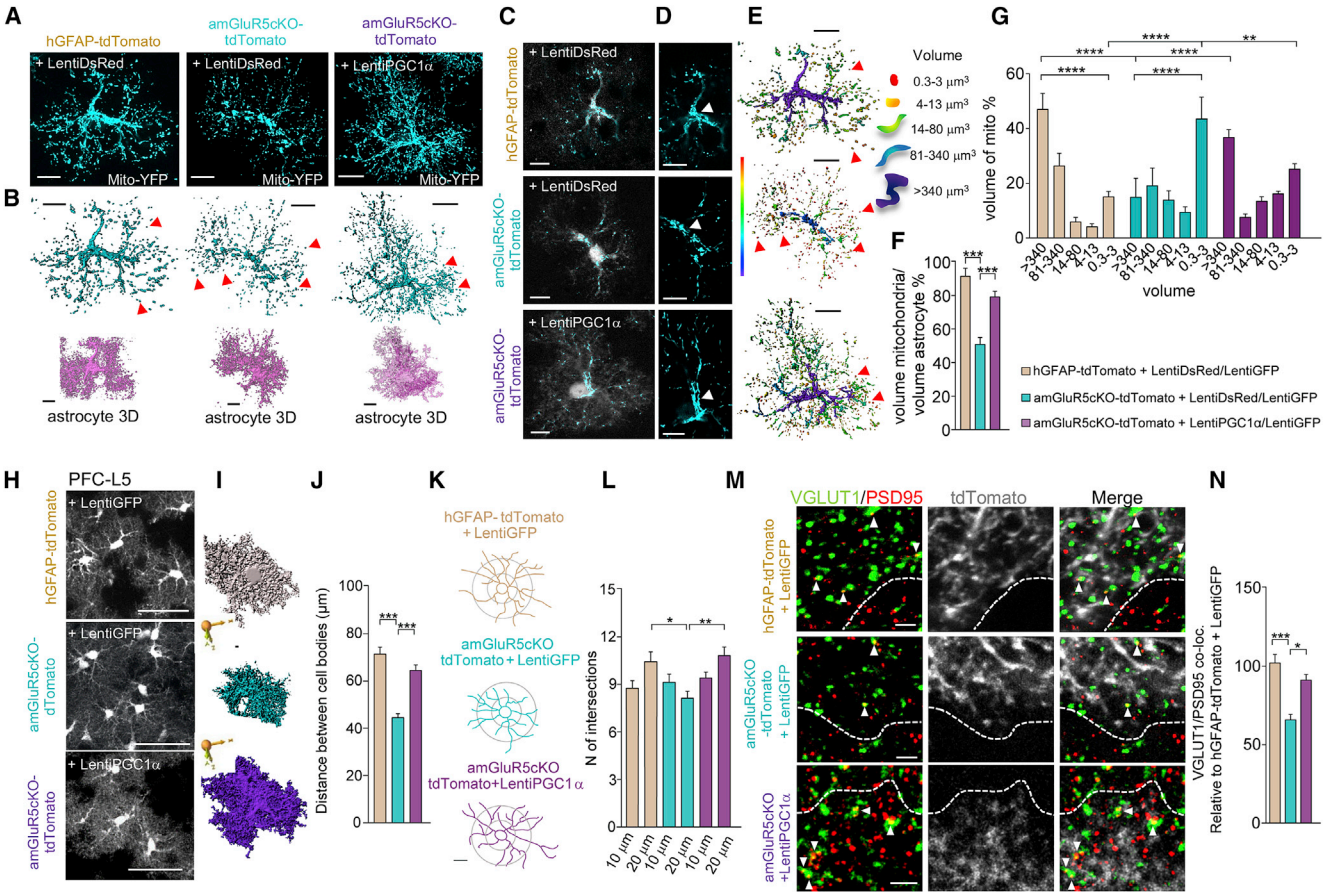

Figure 7. Re-expression of PGC-1α in mGluR5-deficient astrocytes restores the dysmorphogenesis of the mitochondrial network and astrocytes, and has positive effects on synapse formation

(A) Confocal sections of mitochondria in L5 tdTomato astrocytes visualized with IUE of mitoYFP and mTAGBFP2. Scale bar: 10 μm.

(B) Rendering of the three reconstructed astrocytes and mito networks shown in (A). Arrowheads indicate some of the fragmented mito (0.3–3 mm^3) highlighted in (E). Scale bar: 10 μm.

(C and D) Single confocal planes from the images shown in (A). Scale bar: 10 μm.

(E) Rendering of the three reconstructed mito networks shown in (A) showing pseudocolor-coded representation of volume/sphericity. Scale bar: 10 μm.

(F) Quantification of mito occupation in astrocytes on P40. ***$p < 0.001$ (n = 3–4 mice in each group; one-way ANOVA followed by Bonferroni's post hoc correction).

(G) Quantification of the distribution of mito morphology. **$p < 0.01$, ****$p < 0.0001$ (n = 2–3 mice in each group; one-way ANOVA followed by Bonferroni's post hoc correction).

(H) Confocal sections of $tdTomato^+$ astrocytes on P40. Scale bar: 50 μm.

(I) Representative 3D surface rendering showing the volume reconstruction of cortical L5 astrocytes. Scale bar: 10 μm.

(J) Distance between cell bodies of $tdTomato^+$ astrocytes. ***$p < 0.001$ (n = 4 mice in each group; one-way ANOVA followed by Bonferroni's post hoc correction).

(K and L) Sholl analysis of $tdTomato^+$ astrocyte. Scale bar: 10 μm. *$p < 0.05$, **$p < 0.01$ (n = 4 mice in each group; one-way ANOVA followed by Bonferroni's post hoc correction).

(M) Confocal sections of intra-cortical excitatory synapses (VGLUT1, green; PSD95, red) inside the tdTomato astrocyte territory in L5 PFC on P40. Scale bar: 2 μm. Dotted lines show astrocyte boundaries, and arrowheads mark co-localized synaptic puncta.

(N) Quantification of co-localized intra-cortical puncta in the tdTomato astrocyte territories in L5 of the PFC on P40. *$p < 0.05$, ***$p < 0.001$ (n = 3–4 mice each group; one-way ANOVA followed by Bonferroni's post hoc correction).

All error bars represent mean values ± SEM.

of mGluR5 regulates intracellular Ca^{2+} dynamics (Buscemi et al., 2017) and signaling to mTOR (Hou and Klann, 2004; Ronesi and Huber, 2008; Huber et al., 2015). We found that the efficiency of mito biogenesis in developing astrocytes is modulated by mGluR5 signaling via the modulation of PGC-1α levels and global changes in mito structure.

Our model strongly suggests that mGluR5 signaling in developing astrocytes modifies the rate of mito biogenesis, and therefore that mGluR5 in astrocytes monitors glutamatergic synaptic activity and adapts astrocytic energy demands during the first 2 post-natal weeks to support excitatory synaptogenesis. The events coupling the monitoring of synaptic activity by mGluR5

and increasing mito biogenesis seem to be temporally correlated in developing astrocytes, in which the levels of mGluR5 abruptly decrease when those of PGC-1α are reaching their peak during the third post-natal week. Consistently, we found that the activation of mGluR5 increases PGC-1α levels by activating mTOR signaling, as previously suggested in neuronal cells (Ronesi and Huber, 2008). The involvement of mGluR5 signaling in astrocytes also suggests that its ability to modulate mito occupancy must begin early in post-natal development, before the transition from proliferation to morphological and functional maturation occurs because the loss of mGluR5 prolongs the proliferation and delays the maturation of astrocytes. By showing that PGC-1α levels are controlled by mGluR5, and that the re-expression of PGC-1α in newly formed astrocytes carrying the *mGluR5* deletion significantly improves the astrocytic maturation, our data suggest that mGluR5 signaling acts as critical modulator of mito biogenesis and integrates synaptic signals coming from glutamatergic activity in order to stop proliferation and to promote astrocyte maturation. The metabolic capacity and morphogenesis of astrocytes may therefore be induced in a coordinated manner by neurons, as recently proposed by others (Morel et al., 2014; Ge et al., 2012).

Another implication of this study is that mito biogenesis in astrocytes is required for the correct post-natal formation and maturation of synapses. Our *in vivo* analyses demonstrate that PGC-1α deficiency in astrocytes directly affects the formation and function of cortical excitatory synapses, and suggest that defective mito content in developing astrocytes affects synaptic development in neurons. The cell dysfunctions in developing astrocytes that underlie defects in synaptic development are still unknown but may include dysregulation of the normal functions of astrocytes in the developing cortex, such as the regulation of lactate and ATP or of ionic and/or neurotransmitters homeostasis, synaptic pruning, or the provision of metabolites and synaptogenic factors (Petrelli and Bezzi, 2016, 2020; Liddelow and Barres, 2015). Our findings emphasize the importance of astrocyte dysfunction during post-natal development and offer an alternative mechanistic explanation for the synaptic defects characterizing neurodevelopmental disorders, such as autism spectrum disorders, and neuropsychiatric disorders, such as schizophrenia (Karayiorgou et al., 2010; Bariselli et al., 2016; Vicidomini et al., 2017). Furthermore, they support the hypothesis that the pathways governed by PGC-1α and astrocytic mito biogenesis may represent new targets for interventions aimed at improving defective synaptogenesis in these disorders.

STAR★METHODS

Detailed methods are provided in the online version of this paper and include the following:

SUPPLEMENTAL INFORMATION

Supplemental information can be found online at https://doi.org/10.1016/j.celrep.2021.108952.

ACKNOWLEDGMENTS

We would like to thank Margarita Beherens (Salk Institute for the Biological Sciences, USA) for the mGluR5$^{loxp/loxp}$ mice; Carolina Gonçalves for her technical support and her help with the immunohistochemistry experiments; Maria Rey for producing the lentiviral vector; Frank Kirchhoff (University of Saarland, Germany) for the hGFAP-CFP mice; and Marco Vigna Graphic Design for assistance in designing, developing, and reviewing graphics and artwork. This study was supported by grants from the Swiss National Foundation NCCR "Synapsy" (51NF40-158776), "Transcure" (51NF6240-16), and SNFS (26074366) (to P.B.).

AUTHOR CONTRIBUTIONS

T.Z., F.P., J.R, E.C.D.O.F., T.L.L., F.P., M.S., and P.B. performed the experiments and related analyses. N.D. designed the PGC1α plasmids and produced the lentiviral vectors. P.B. wrote the manuscript, which was discussed and approved by all of the authors.

DECLARATION OF INTERESTS

The authors declare no competing interests.

Received: April 28, 2020
Revised: January 10, 2021
Accepted: March 15, 2021
Published: April 13, 2021

SUPPORTING CITATIONS

The following references appear in the supplemental information: Cui et al. (2014); Giese et al. (2012); Ortolano et al. (2008); Skliris et al. (2015); Sobecki et al. (2016); Xu et al. (2009).

REFERENCES

Agathocleous, M., Love, N.K., Randlett, O., Harris, J.J., Liu, J., Murray, A.J., and Harris, W.A. (2012). Metabolic differentiation in the embryonic retina. Nat. Cell Biol. *14*, 859–864.

Agostini, M., Romeo, F., Inoue, S., Niklison-Chirou, M.V., Elia, A.J., Dinsdale, D., Morone, N., Knight, R.A., Mak, T.W., and Melino, G. (2016). Metabolic reprogramming during neuronal differentiation. Cell Death Differ. *23*, 1502–1514.

Allen, N.J., and Eroglu, C. (2017). Cell Biology of Astrocyte-Synapse Interactions. Neuron *96*, 697–708.

Azzalin, A., Brambilla, F., Arbustini, E., Basello, K., Speciani, A., Mauri, P., Bezzi, P., and Magrassi, L. (2020). A new pathway promotes adaptation of human glioblastoma cells to glucose starvation. Cells *18*, 1249.

Bandeira, F., Lent, R., and Herculano-Houzel, S. (2009). Changing numbers of neuronal and non-neuronal cells underlie postnatal brain growth in the rat. Proc. Natl. Acad. Sci. USA *106*, 14108–14113.

Bariselli, S., Tzanoulinou, S., Glangetas, C., Prévost-Solié, C., Pucci, L., Viguié, J., Bezzi, P., O'Connor, E.C., Georges, F., Lüscher, C., and Bellone, C. (2016). SHANK3 controls maturation of social reward circuits in the VTA. Nat. Neurosci. *19*, 926–934.

Barnes, S.A., Pinto-Duarte, A., Kappe, A., Zembrzycki, A., Metzler, A., Mukamel, E.A., Lucero, J., Wang, X., Sejnowski, T.J., Markou, A., and Behrens, M.M. (2015). Disruption of mGluR5 in parvalbumin-positive interneurons induces core features of neurodevelopmental disorders. Mol. Psychiatry *20*, 1161–1172.

Beckervordersandforth, R., Ebert, B., Schäffner, I., Moss, J., Fiebig, C., Shin, J., Moore, D.L., Ghosh, L., Trinchero, M.F., Stockburger, C., et al. (2017). Role of Mitochondrial Metabolism in the Control of Early Lineage Progression and Aging Phenotypes in Adult Hippocampal Neurogenesis. Neuron *93*, 560–573.e6.

Bezzi, P., Carmignoto, G., Pasti, L., Vesce, S., Rossi, D., Rizzini, B.L., Pozzan, T., and Volterra, A. (1998). Prostaglandins stimulate calcium-dependent glutamate release in astrocytes. Nature *391*, 281–285.

Boisvert, M.M., Erikson, G.A., Shokhirev, M.N., and Allen, N.J. (2018). The Aging Astrocyte Transcriptome from Multiple Regions of the Mouse Brain. Cell Rep. *22*, 269–285.

Bouzier-Sore, A.K., and Pellerin, L. (2013). Unraveling the complex metabolic nature of astrocytes. Front. Cell. Neurosci. *7*, 179.

Buscemi, L., Ginet, V., Lopatar, J., Montana, V., Pucci, L., Spagnuolo, P., Zehnder, T., Grubišic, V., Truttman, A., Sala, C., et al. (2017). Homer1 Scaffold Proteins Govern Ca2+ Dynamics in Normal and Reactive Astrocytes. Cereb. Cortex *27*, 2365–2384.

Cahoy, J.D., Emery, B., Kaushal, A., Foo, L.C., Zamanian, J.L., Christopherson, K.S., Xing, Y., Lubischer, J.L., Krieg, P.A., Krupenko, S.A., et al. (2008). A transcriptome database for astrocytes, neurons, and oligodendrocytes: a new resource for understanding brain development and function. J. Neurosci. *28*, 264–278.

Cai, Z., Schools, G.P., and Kimelberg, H.K. (2000). Metabotropic glutamate receptors in acutely isolated hippocampal astrocytes: developmental changes of mGluR5 mRNA and functional expression. Glia *29*, 70–80.

Calì, C., Tauffenberger, A., and Magistretti, P. (2019). The Strategic Location of Glycogen and Lactate: From Body Energy Reserve to Brain Plasticity. Front. Cell. Neurosci. *13*, 82.

Cathala, L., Holderith, N.B., Nusser, Z., DiGregorio, D.A., and Cull-Candy, S.G. (2005). Changes in synaptic structure underlie the developmental speeding of AMPA receptor-mediated EPSCs. Nat. Neurosci. *8*, 1310–1318.

Cheng, A., Wan, R., Yang, J.L., Kamimura, N., Son, T.G., Ouyang, X., Luo, Y., Okun, E., and Mattson, M.P. (2012). Involvement of PGC-1α in the formation and maintenance of neuronal dendritic spines. Nat. Commun. *3*, 1250.

Colin, A., Faideau, M., Dufour, N., Auregan, G., Hassig, R., Andrieu, T., Brouillet, E., Hantraye, P., Bonvento, G., and Déglon, N. (2009). Engineered lentiviral vector targeting astrocytes in vivo. Glia *57*, 667–679.

Cui, W., Mizukami, H., Yanagisawa, M., Aida, T., Nomura, M., Isomura, Y., Takayanagi, R., Ozawa, K., Tanaka, K., and Aizawa, H. (2014). Glial dysfunction in the mouse habenula causes depressive-like behaviors and sleep disturbance. J. Neurosci. *34*, 16273–16285.

Cunningham, J.T., Rodgers, J.T., Arlow, D.H., Vazquez, F., Mootha, V.K., and Puigserver, P. (2007). mTOR controls mitochondrial oxidative function through a YY1-PGC-1alpha transcriptional complex. Nature *450*, 736–740.

Czubryt, M.P., McAnally, J., Fishman, G.I., and Olson, E.N. (2003). Regulation of peroxisome proliferator-activated receptor gamma coactivator 1 alpha (PGC-1 alpha) and mitochondrial function by MEF2 and HDAC5. Proc. Natl. Acad. Sci. USA *100*, 1711–1716.

Dawson, M.R.L., Levine, J.M., and Reynolds, R. (2000). NG2-expressing cells in the central nervous system: are they oligodendroglial progenitors? J. Neurosci. Res. *61*, 471–479.

Dawson, M.R.L., Polito, A., Levine, J.M., and Reynolds, R. (2003). NG2-expressing glial progenitor cells: an abundant and widespread population of cycling cells in the adult rat CNS. Mol. Cell. Neurosci. *24*, 476–488.

Diebold, L.P., Gil, H.J., Gao, P., Martinez, C.A., Weinberg, S.E., and Chandel, N.S. (2019). Mitochondrial complex III is necessary for endothelial cell proliferation during angiogenesis. Nat. Metab. *1*, 158–171.

Farhy-Tselnicker, I., van Casteren, A.C.M., Lee, A., Chang, V.T., Aricescu, A.R., and Allen, N.J. (2017). Astrocyte-Secreted Glypican 4 Regulates Release of Neuronal Pentraxin 1 from Axons to Induce Functional Synapse Formation. Neuron *96*, 428–445.e13.

Finck, B.N., and Kelly, D.P. (2006). PGC-1 coactivators: inducible regulators of energy metabolism in health and disease. J. Clin. Invest. *116*, 615–622.

Freeman, M.R. (2010). Specification and morphogenesis of astrocytes. Science *330*, 774–778.

Göbel, J., Engelhardt, E., Pelzer, P., Sakthivelu, V., Jahn, H.M., Jevtic, M., Folz-Donahue, K., Kukat, C., Schauss, A., Frese, C.K., et al. (2020). Mitochondria-Endoplasmic Reticulum Contacts in Reactive Astrocytes Promote Vascular Remodeling. Cell Metab. *31*, 791–808.e8.

Ge, W.P., Miyawaki, A., Gage, F.H., Jan, Y.N., and Jan, L.Y. (2012). Local generation of glia is a major astrocyte source in postnatal cortex. Nature *484*, 376–380.

Giese, S., Hossain, H., Markmann, M., Chakraborty, T., Tchatalbachev, S., Guillou, F., Bergmann, M., Failing, K., Weider, K., and Brehm, R. (2012). Sertoli-cell-specific knockout of connexin 43 leads to multiple alterations in testicular gene expression in prepubertal mice. Dis. Model. Mech. *5*, 895–913.

Gotoh, K., Morisaki, T., Setoyama, D., Sasaki, K., Yagi, M., Igami, K., Mizuguchi, S., Uchiumi, T., Fukui, Y., and Kang, D. (2018). Mitochondrial p32/C1qbp Is a Critical Regulator of Dendritic Cell Metabolism and Maturation. Cell Rep. *25*, 1800–1815.e4.

Hackenbrock, C.R. (1968). Ultrastructural bases for metabolically linked mechanical activity in mitochondria. II. Electron transport-linked ultrastructural transformations in mitochondria. J. Cell Biol. *37*, 345–369.

Hasel, P., Dando, O., Jiwaji, Z., Baxter, P., Todd, A.C., Heron, S., Márkus, N.M., McQueen, J., Hampton, D.W., Torvell, M., et al. (2017). Neurons and neuronal activity control gene expression in astrocytes to regulate their development and metabolism. Nat. Commun. *8*, 15132.

Herzig, S., Long, F., Jhala, U.S., Hedrick, S., Quinn, R., Bauer, A., Rudolph, D., Schutz, G., Yoon, C., Puigserver, P., et al. (2001). CREB regulates hepatic gluconeogenesis through the coactivator PGC-1. Nature *413*, 179–183.

Hirrlinger, P.G., Scheller, A., Braun, C., Quintela-Schneider, M., Fuss, B., Hirrlinger, J., and Kirchhoff, F. (2005). Expression of reef coral fluorescent proteins in the central nervous system of transgenic mice. Mol. Cell. Neurosci. *30*, 291–303.

Hirrlinger, P.G., Scheller, A., Braun, C., Hirrlinger, J., and Kirchhoff, F. (2006). Temporal control of gene recombination in astrocytes by transgenic expression of the tamoxifen-inducible DNA recombinase variant CreERT2. Glia *54*, 11–20.

Hock, M.B., and Kralli, A. (2009). Transcriptional control of mitochondrial biogenesis and function. Annu. Rev. Physiol. *71*, 177–203.

Homem, C.C.F., Steinmann, V., Burkard, T.R., Jais, A., Esterbauer, H., and Knoblich, J.A. (2014). Ecdysone and mediator change energy metabolism to terminate proliferation in Drosophila neural stem cells. Cell *158*, 874–888.

Hottinger, A.F., Azzouz, M., Déglon, N., Aebischer, P., and Zurn, A.D. (2000). Complete and long-term rescue of lesioned adult motoneurons by lentiviral-mediated expression of glial cell line-derived neurotrophic factor in the facial nucleus. J. Neurosci. *20*, 5587–5593.

Hou, L., and Klann, E. (2004). Activation of the phosphoinositide 3-kinase-Akt-mammalian target of rapamycin signaling pathway is required for metabotropic glutamate receptor-dependent long-term depression. J. Neurosci. *24*, 6352–6361.

Huber, K.M., Klann, E., Costa-Mattioli, M., and Zukin, R.S. (2015). Dysregulation of Mammalian Target of Rapamycin Signaling in Mouse Models of Autism. J. Neurosci. *35*, 13836–13842.

Humbel, M., Ramosaj, M., Zimmer, V., Regio, S., Aeby, L., Moser, S., Boizot, A., Sipion, M., Rey, M., and Déglon, N. (2021). Maximizing lentiviral vector gene transfer in the CNS. Gene Ther. *28*, 75–88.

Ignatenko, O., Chilov, D., Paetau, I., de Miguel, E., Jackson, C.B., Capin, G., Paetau, A., Terzioglu, M., Euro, L., and Suomalainen, A. (2018). Loss of mtDNA activates astrocytes and leads to spongiotic encephalopathy. Nat. Commun. *9*, 70.

Jiang, H., Kang, S.U., Zhang, S., Karuppagounder, S., Xu, J., Lee, Y.K., Kang, B.G., Lee, Y., Zhang, J., Pletnikova, O., et al. (2016). Adult Conditional Knockout of PGC-1α Leads to Loss of Dopamine Neurons. eNeuro *3*, 8.

Kamei, Y., Ohizumi, H., Fujitani, Y., Nemoto, T., Tanaka, T., Takahashi, N., Kawada, T., Miyoshi, M., Ezaki, O., and Kakizuka, A. (2003). PPARgamma coactivator 1beta/ERR ligand 1 is an ERR protein ligand, whose expression induces a high-energy expenditure and antagonizes obesity. Proc. Natl. Acad. Sci. USA *100*, 12378–12383.

Karayiorgou, M., Simon, T.J., and Gogos, J.A. (2010). 22q11.2 microdeletions: linking DNA structural variation to brain dysfunction and schizophrenia. Nat. Rev. Neurosci. *11*, 402–416.

Khacho, M., Clark, A., Svoboda, D.S., Azzi, J., MacLaurin, J.G., Meghaizel, C., Sesaki, H., Lagace, D.C., Germain, M., Harper, M.E., et al. (2016). Mitochondrial Dynamics Impacts Stem Cell Identity and Fate Decisions by Regulating a Nuclear Transcriptional Program. Cell Stem Cell *19*, 232–247.

Khacho, M., Harris, R., and Slack, R.S. (2019). Mitochondria as central regulators of neural stem cell fate and cognitive function. Nat. Rev. Neurosci. *20*, 34–48.

Knobloch, M., Braun, S.M.G., Zurkirchen, L., von Schoultz, C., Zamboni, N., Araúzo-Bravo, M.J., Kovacs, W.J., Karalay, O., Suter, U., Machado, R.A.C., et al. (2013). Metabolic control of adult neural stem cell activity by Fasn-dependent lipogenesis. Nature *493*, 226–230.

Kozorovitskiy, Y., Peixoto, R., Wang, W., Saunders, A., and Sabatini, B.L. (2015). Neuromodulation of excitatory synaptogenesis in striatal development. eLife *4*, 18.

LeBleu, V.S., O'Connell, J.T., Gonzalez Herrera, K.N., Wikman, H., Pantel, K., Haigis, M.C., de Carvalho, F.M., Damascena, A., Domingos Chinen, L.T., Rocha, R.M., et al. (2014). PGC-1α mediates mitochondrial biogenesis and oxidative phosphorylation in cancer cells to promote metastasis. Nat. Cell Biol. *16*, 992–1003, 1–15.

Lelliott, C.J., Medina-Gomez, G., Petrovic, N., Kis, A., Feldmann, H.M., Bjursell, M., Parker, N., Curtis, K., Campbell, M., Hu, P., et al. (2006). Ablation of PGC-1beta results in defective mitochondrial activity, thermogenesis, hepatic function, and cardiac performance. PLoS Biol. *4*, e369.

Leone, T.C., Lehman, J.J., Finck, B.N., Schaeffer, P.J., Wende, A.R., Boudina, S., Courtois, M., Wozniak, D.F., Sambandam, N., Bernal-Mizrachi, C., et al. (2005). PGC-1alpha deficiency causes multi-system energy metabolic derangements: muscle dysfunction, abnormal weight control and hepatic steatosis. PloS Biol. *3*, e101.

Levine, J.M., Reynolds, R., and Fawcett, J.W. (2001). The oligodendrocyte precursor cell in health and disease. Trends Neurosci. *24*, 39–47.

Lewis, T.L., Jr., Kwon, S.K., Lee, A., Shaw, R., and Polleux, F. (2018). MFF-dependent mitochondrial fission regulates presynaptic release and axon branching by limiting axonal mitochondria size. Nat. Commun. *9*, 5008.

Li, Z., Okamoto, K., Hayashi, Y., and Sheng, M. (2004). The importance of dendritic mitochondria in the morphogenesis and plasticity of spines and synapses. Cell *119*, 873–887.

Liddelow, S., and Barres, B. (2015). SnapShot: Astrocytes in Health and Disease. Cell *162*, 1170–1170.e1.

Lin, J., Wu, P.H., Tarr, P.T., Lindenberg, K.S., St-Pierre, J., Zhang, C.Y., Mootha, V.K., Jäger, S., Vianna, C.R., Reznick, R.M., et al. (2004). Defects in adaptive energy metabolism with CNS-linked hyperactivity in PGC-1alpha null mice. Cell *119*, 121–135.

Lin, J., Handschin, C., and Spiegelman, B.M. (2005). Metabolic control through the PGC-1 family of transcription coactivators. Cell Metab. *1*, 361–370.

Magistretti, P.J., and Allaman, I. (2018). Lactate in the brain: from metabolic end-product to signalling molecule. Nat. Rev. Neurosci. *19*, 235–249.

Magistretti, P., Grenningloh, G., and Allaman, I. (2015). Role of glycogen-derived lactate in synaptic plasticity and memory. J. Neurochem. *134*, 57.

Marchaland, J., Calì, C., Voglmaier, S.M., Li, H., Regazzi, R., Edwards, R.H., and Bezzi, P. (2008). Fast subplasma membrane Ca2+ transients control exo-endocytosis of synaptic-like microvesicles in astrocytes. J. Neurosci. *28*, 9122–9132.

Medeiros, D.M. (2008). Assessing mitochondria biogenesis. Methods *46*, 288–294.

Merienne, N., Le Douce, J., Faivre, E., Déglon, N., and Bonvento, G. (2013). Efficient gene delivery and selective transduction of astrocytes in the mammalian brain using viral vectors. Front. Cell. Neurosci. *7*, 106.

Morel, L., Higashimori, H., Tolman, M., and Yang, Y. (2014). VgluT1+ neuronal glutamatergic signaling regulates postnatal developmental maturation of cortical protoplasmic astroglia. J. Neurosci. *34*, 10950–10962.

Morita, M., Gravel, S.P., Chénard, V., Sikström, K., Zheng, L., Alain, T., Gandin, V., Avizonis, D., Arguello, M., Zakaria, C., et al. (2013). mTORC1 controls mitochondrial activity and biogenesis through 4E-BP-dependent translational regulation. Cell Metab. *18*, 698–711.

Motori, E., Puyal, J., Toni, N., Ghanem, A., Angeloni, C., Malaguti, M., Cantelli-Forti, G., Berninger, B., Conzelmann, K.K., Götz, M., et al. (2013). Inflammation-induced alteration of astrocyte mitochondrial dynamics requires autophagy for mitochondrial network maintenance. Cell Metab. *18*, 844–859.

Nishiyama, A., Watanabe, M., Yang, Z., and Bu, J. (2002). Identity, distribution, and development of polydendrocytes: NG2-expressing glial cells. J. Neurocytol. *31*, 437–455.

Ortolano, S., Di Pasquale, G., Crispino, G., Anselmi, F., Mammano, F., and Chiorini, J.A. (2008). Coordinated control of connexin 26 and connexin 30 at the regulatory and functional level in the inner ear. Proc. Natl. Acad. Sci. USA *105*, 18776–18781.

Pannasch, U., Freche, D., Dallérac, G., Ghézali, G., Escartin, C., Ezan, P., Cohen-Salmon, M., Benchenane, K., Abudara, V., Dufour, A., et al. (2014). Connexin 30 sets synaptic strength by controlling astroglial synapse invasion. Nat. Neurosci. *17*, 549–558.

Peters, A. (2004). A fourth type of neuroglial cell in the adult central nervous system. J. Neurocytol. *33*, 345–357.

Petrelli, F., and Bezzi, P. (2016). Novel insights into gliotransmitters. Curr. Opin. Pharmacol. *26*, 138–145.

Petrelli, F., and Bezzi, P. (2018). mGlu5-mediated signalling in developing astrocyte and the pathogenesis of autism spectrum disorders. Curr. Opin. Neurobiol. *48*, 139–145.

Petrelli, F., Dallérac, G., Pucci, L., Calì, C., Zehnder, T., Sultan, S., Lecca, S., Chicca, A., Ivanov, A., Asensio, C.S., et al. (2020). Dysfunction of homeostatic control of dopamine by astrocytes in the developing prefrontal cortex leads to cognitive impairments. Mol. Psychiatry *25*, 732–749.

Pooya, S., Liu, X., Kumar, V.B.S., Anderson, J., Imai, F., Zhang, W., Ciraolo, G., Ratner, N., Setchell, K.D.R., Yoshida, Y., et al. (2014). The tumour suppressor LKB1 regulates myelination through mitochondrial metabolism. Nat. Commun. *5*, 4993.

Prada, I., Marchaland, J., Podini, P., Magrassi, L., D'Alessandro, R., Bezzi, P., and Meldolesi, J. (2011). REST/NRSF governs the expression of dense-core vesicle gliosecretion in astrocytes. J. Cell Biol. *193*, 537–549.

Puigserver, P., and Spiegelman, B.M. (2003). Peroxisome proliferator-activated receptor-gamma coactivator 1 alpha (PGC-1 alpha): transcriptional coactivator and metabolic regulator. Endocr. Rev. *24*, 78–90.

Raponi, E., Agenes, F., Delphin, C., Assard, N., Baudier, J., Legraverend, C., and Deloulme, J.C. (2007). S100B expression defines a state in which GFAP-expressing cells lose their neural stem cell potential and acquire a more mature developmental stage. Glia *55*, 165–177.

Richetin, K., Steullet, P., Pachoud, M., Perbet, R., Parietti, E., Maheswaran, M., Eddarkaoui, S., Bégard, S., Pythoud, C., Rey, M., et al. (2020). Tau accumulation in astrocytes of the dentate gyrus induces neuronal dysfunction and memory deficits in Alzheimer's disease. Nat. Neurosci. *23*, 1567–1579.

Ronesi, J.A., and Huber, K.M. (2008). Homer interactions are necessary for metabotropic glutamate receptor-induced long-term depression and translational activation. J. Neurosci. *28*, 543–547.

Sakers, K., and Eroglu, C. (2019). Control of neural development and function by glial neuroligins. Curr. Opin. Neurobiol. *57*, 163–170.

Scarpulla, R.C. (2011). Metabolic control of mitochondrial biogenesis through the PGC-1 family regulatory network. Biochim. Biophys. Acta *1813*, 1269–1278.

Skliris, A., Papadaki, O., Kafasla, P., Karakasiliotis, I., Hazapis, O., Reczko, M., Grammenoudi, S., Bauer, J., and Kontoyiannis, D.L. (2015). Neuroprotection requires the functions of the RNA-binding protein HuR. Cell Death Differ. *22*, 703–718.

Sobecki, M., Mrouj, K., Camasses, A., Parisis, N., Nicolas, E., Llères, D., Gerbe, F., Prieto, S., Krasinska, L., David, A., et al. (2016). The cell proliferation antigen Ki-67 organises heterochromatin. eLife *5*, e13722.

Stogsdill, J.A., Ramirez, J., Liu, D., Kim, Y.H., Baldwin, K.T., Enustun, E., Ejikeme, T., Ji, R.R., and Eroglu, C. (2017). Astrocytic neuroligins control astrocyte morphogenesis and synaptogenesis. Nature *551*, 192–197.

Sun, W., McConnell, E., Pare, J.F., Xu, Q., Chen, M., Peng, W., Lovatt, D., Han, X., Smith, Y., and Nedergaard, M. (2013). Glutamate-dependent neuroglial calcium signaling differs between young and adult brain. Science *339*, 197–200.

Supplie, L.M., Düking, T., Campbell, G., Diaz, F., Moraes, C.T., Götz, M., Hamprecht, B., Boretius, S., Mahad, D., and Nave, K.A. (2017). Respiration-Deficient Astrocytes Survive As Glycolytic Cells *In Vivo*. J. Neurosci. *37*, 4231–4242.

Taschenberger, H., and von Gersdorff, H. (2000). Fine-tuning an auditory synapse for speed and fidelity: developmental changes in presynaptic waveform, EPSC kinetics, and synaptic plasticity. J. Neurosci. *20*, 9162–9173.

Tran, M.T., Zsengeller, Z.K., Berg, A.H., Khankin, E.V., Bhasin, M.K., Kim, W., Clish, C.B., Stillman, I.E., Karumanchi, S.A., Rhee, E.P., and Parikh, S.M. (2016). PGC1α drives NAD biosynthesis linking oxidative metabolism to renal protection. Nature *531*, 528–532.

Vayssière, J.L., Cordeau-Lossouarn, L., Larcher, J.C., Basseville, M., Gros, F., and Croizat, B. (1992). Participation of the mitochondrial genome in the differentiation of neuroblastoma cells. In Vitro Cell. Dev. Biol. *28A*, 763–772.

Vicidomini, C., Ponzoni, L., Lim, D., Schmeisser, M.J., Reim, D., Morello, N., Orellana, D., Tozzi, A., Durante, V., Scalmani, P., et al. (2017). Pharmacological enhancement of mGlu5 receptors rescues behavioral deficits in SHANK3 knock-out mice. Mol. Psychiatry *22*, 689–702.

Volk, L.J., Pfeiffer, B.E., Gibson, J.R., and Huber, K.M. (2007). Multiple Gq-coupled receptors converge on a common protein synthesis-dependent long-term depression that is affected in fragile X syndrome mental retardation. J. Neurosci. *27*, 11624–11634.

Wall, M.J., Robert, A., Howe, J.R., and Usowicz, M.M. (2002). The speeding of EPSC kinetics during maturation of a central synapse. Eur. J. Neurosci. *15*, 785–797.

Weber, B., and Barros, L.F. (2015). The Astrocyte: Powerhouse and Recycling Center. Cold Spring Harb. Perspect. Biol. *7*, 15.

Weng, Q., Wang, J., Wang, J., He, D., Cheng, Z., Zhang, F., Verma, R., Xu, L., Dong, X., Liao, Y., et al. (2019). Single-Cell Transcriptomics Uncovers Glial Progenitor Diversity and Cell Fate Determinants during Development and Gliomagenesis. Cell Stem Cell *24*, 707–723.e8.

Wu, Z., Puigserver, P., Andersson, U., Zhang, C., Adelmant, G., Mootha, V., Troy, A., Cinti, S., Lowell, B., Scarpulla, R.C., and Spiegelman, B.M. (1999). Mechanisms controlling mitochondrial biogenesis and respiration through the thermogenic coactivator PGC-1. Cell *98*, 115–124.

Xing, F., Luan, Y., Cai, J., Wu, S., Mai, J., Gu, J., Zhang, H., Li, K., Lin, Y., Xiao, X., et al. (2017). The Anti-Warburg Effect Elicited by the cAMP-PGC1α Pathway Drives Differentiation of Glioblastoma Cells into Astrocytes. Cell Rep. *18*, 468–481.

Xu, J., Zhu, Y., Contractor, A., and Heinemann, S.F. (2009). mGluR5 has a critical role in inhibitory learning. J. Neurosci. *29*, 3676–3684.

Yao, C.H., Wang, R., Wang, Y., Kung, C.P., Weber, J.D., and Patti, G.J. (2019). Mitochondrial fusion supports increased oxidative phosphorylation during cell proliferation. eLife *8*, 19.

Zhang, Y., Sloan, S.A., Clarke, L.E., Caneda, C., Plaza, C.A., Blumenthal, P.D., Vogel, H., Steinberg, G.K., Edwards, M.S.B., Li, G., et al. (2016). Purification and Characterization of Progenitor and Mature Human Astrocytes Reveals Transcriptional and Functional Differences with Mouse. Neuron *89*, 37–53.

Zheng, X., Boyer, L., Jin, M., Mertens, J., Kim, Y., Ma, L., Ma, L., Hamm, M., Gage, F.H., and Hunter, T. (2016). Metabolic reprogramming during neuronal differentiation from aerobic glycolysis to neuronal oxidative phosphorylation. eLife *5*, 25.

Zheng, H., Yu, W.M., Shen, J., Kang, S., Hambardzumyan, D., Li, J.Y., Shen, Y., Kenney, A.M., Chen, J., and Qu, C.K. (2018). Mitochondrial oxidation of the carbohydrate fuel is required for neural precursor/stem cell function and postnatal cerebellar development. Sci. Adv. *4*, eaat2681.

Zong, H., Ren, J.M., Young, L.H., Pypaert, M., Mu, J., Birnbaum, M.J., and Shulman, G.I. (2002). AMP kinase is required for mitochondrial biogenesis in skeletal muscle in response to chronic energy deprivation. Proc. Natl. Acad. Sci. USA *99*, 15983–15987.

STAR★METHODS

KEY RESOURCES TABLE

REAGENT or RESOURCE	SOURCE	IDENTIFIER
Antibodies		
Mouse anti-Glutamine Synthetase	Merck Millipore	RRID: AB_2314617
Rabbit anti-GFAP	Merck Millipore	RRID:AB_94844
Rabbit anti Ki67	Abcam	RRID:AB_443209
Mouse anti-NeuN	Merck Millipore	RRID:AB_2298772
Guinea Pig anti-Vglut1	Synaptic System	RRID:AB_887878
Rabbit anti-Vglut2	Synaptic System	RRID:AB_887883
Mouse anti-PSD95	Merck Millipore	RRID:AB_2092365
Rat anti-BrdU	Abcam	RRID:AB_305426
Rabbit anti-Cleaved Casp3	BioConcept	RRID:AB_2070042
Rat anti-CTIP2	Abcam	RRID:AB_2064130
Mouse anti-mTOR	Cell signaling	RRID:AB_1904056
Rabbit anti-P-mTOR (Ser2448)	Cell signaling	RRID:AB_330970
Mouse anti-PGC1α	Merck Millipore	RRID:AB_2237237
Mouse anti-αTubulin	Santa Cruz	RRID:AB_628408
Rabbit anti-NG2	Abcam	RRID:AB_91789
Mouse anti-S100b	Abcam	RRID:AB_477499
Goat anti-mouse Alexa Fluor 488	Invitrogen	RRID:AB_2534088
Goat anti-mouse Alexa Fluor 555	Invitrogen	RRID:AB_2633276
Goat anti-rabbit Alexa Fluor 488	Invitrogen	RRID:AB_2576217
Goat anti-rabbit Alexa Fluor cy3	Invitrogen	RRID:AB_2534029
Goat anti-Guinea Pig Alexa 488	Invitrogen	RRID:AB_2534117
Donkey anti-Rat Alexa Fluor 488	Invitrogen	RRID:AB_2535794
Donkey anti-Rat IgG (H+L) Alexa 488	Invitrogen	RRID:AB_2535794
Goat anti-mouse Fluor cy5	Jackson Immuno Research Lab	RRID:AB_2338713
Goat anti-mouse Fluor cy3	Jackson Immuno Research Lab	RRID: AB_2338680
Goat anti-rabbit Fluor cy3	Jackson Immuno Research Lab	RRID:AB_2338006
Goat anti-rabbit IRdye 800 CW	Li-Cor	RRID:AB_621843
Goat anti-rabbit IRdye 680 RD	Li-Cor	RRID:AB_10956166
Goat anti-mouse IRdye 800	Li-Cor	RRID:AB_621842
Goat anti-mouse IRdye 680	Li-Cor	RRID:AB_621840
Bacterial and virus strains		
LentiGFP virus VSVG pseudotype	Laboratory of Nicole Deglon at CHUV Lausanne	Petrelli et al., 2020
LentiPGC1α virus VSVG pseudotype	Laboratory of Nicole Deglon at CHUV Lausanne	N/A
LentiDsRed virus VSVG pseudotype	Laboratory of Nicole Deglon at CHUV Lausanne	N/A
Biological samples		
No biological samples used	N/A	N/A
Chemicals, peptides, and recombinant proteins		
MitoTracker^{R} Green FM	Invitrogen	Cat# M7514
mPEP hydrochloride	R&D Systems	Cat# 1212
(Z)-4-Hydroxytamoxifen	Sigma-Aldrich	Cat# H7904

(*Continued on next page*)

Continued

REAGENT or RESOURCE	SOURCE	IDENTIFIER
5-bromo-2′-deoxyuridine (BrdU)	Sigma-Aldrich	Cat# HY-15910
N-[2-[[[3-(4-Chlorophenyl)-2-propenyl]methylamino]methyl]phenyl]-N-(2-hydroxyethyl)-4-methoxybenzenesulphonamide (KN93)	Sigma-Aldrich	Cat# 422711
Rapamycin	Sigma-Aldrich	Cat# R0395
(RS)-3,5-Dihydroxyphenylglycine (DHPG)	R&D Systems	Cat# 0342
1,2-bis(o-aminophenoxy)ethane-N,N,N′,N′-tetraacetic acid (BAPTA-AM)	Sigma-Aldrich	Cat# 11696
Critical commercial assays		
ATP determination Kit	ThermoFisher	Cat# A22066
L-lactate assay kit	Sigma	Cat# MAK065
Seahorse XFp Mito stress test kit	Seahorse Bioscience, Bucher Biotec AG	Cat# 103010-100
Seahorse XFp Fluxpak kit	Seahorse Bioscience, Bucher Biotec AG	Cat# 103022-100
Deposited data		
No deposited data	N/A	N/A
Experimental models: Cell lines		
No cell lines used	N/A	N/A
Experimental models: Organisms/strains		
Mouse: B6N.129(FVB)-Ppargc1a < tm2.1Brsp > /J Case: **PGC1αLox/Lox**	The Jackson Laboratory	JAX stock #SN9666
Mouse: B6N.129(FVB)-Ppargc1a < tm2.1Brsp > /J Case x Tg(GFAP-cre/ERT2)1Fki x B6.Cg-Gt(ROSA)26Sortm14(CAG-tdTomato)Hze/J: **aPGC1αcKO-tdTomato**	This paper	N/A
Mouse: Tg(GFAP-cre/ERT2)1Fki x B6.Cg-Gt(ROSA)26Sortm14(CAG-tdTomato)Hze/J X mGluR5lox: **amGluR5cKO-tdTomato**	This paper	N/A
Mouse**: mGluR5Lox/Lox**	Laboratory of Margarita Behrens at Salk institute for Biological Studies	Barnes et al., 2015
Mouse: Tg(GFAP-cre/ERT2)1Fki xB6.Cg-Gt(ROSA)26Sortm14(CAG-tdTomato)Hze/J: **hGFAP-tdTomato**	This paper	N/A
Mouse: TgN (hGFAP-ECFP)-GCED: **GFAP-ECFP**	Franck Kirchhoff Lab	Hirrlinger et al., 2005
Mouse: Gt(ROSA)26Sor m14(CAG-tdTomato)Hze/J: **tdTomato**	The Jackson Laboratory	JAX Stock #007914
Oligonucleotides		
Primers for genotyping: See Table S1		N/A
Primers for semiquantitative RT-PCR: See Table S2		N/A
Recombinant DNA		
Plasmid: PiggyBac transposase	Laboratory of Franck Polleux at Columbia University	N/A
Plasmid: PBmTAGBFP2_P2a_mtYFP	Laboratory of Franck Polleux at Columbia University	N/A
Software and algorithms		
IMARIS	Bitplane AG	https://imaris.oxinst.com
GraphPad Prism 8.0.2	GraphPad Software LLC	https://www.graphpad.com
Leica LAS X	Leica systems	https://www.leica-microsystems.com
Fiji/ImageJ	NIH	https://imagej.nih.gov
Adobe Photoshop CS5	Adobe System Incorporated	N/A

RESOURCE AVAILABILITY

Lead contact

Further information and requests for resources and reagents should be directed to and will be fulfilled by the Lead Contact Prof. Paola Bezzi, paola.bezzi@unil.ch

Materials availability

This study did not generate new unique reagents.

Data and code availability

This study did not generate any unique datasets or code.

EXPERIMENTAL MODEL AND SUBJECT DETAILS

Animal experiments were conducted in accordance with ethical guidelines of the Ethics Committee for Animal Experimentation of the Swiss Academy of Medical Sciences (SAMS) and the Swiss Academy of Sciences (SCNAT) and approved by the cantonal animal testing commission ("Service de la consommation et des affaires vétérinaries du Canton Vaud, Lausanne"). All mice were housed with food and water available *ad libitum* in a 12 hour light/dark environment. All animals were sacrificed during the light cycle, and none were involved in previous studies.

Experiments were performed using between 1 and 7 week old mice. hGFAPcre^{ERT2} (B6.Tg(GFAP-cre/ERT2)1Fki), hGFAP-CFP (TgN(hGFAP-ECFP)-GCED) have been obtained from Frank Kirchhoff (Molecular Physiology, University of Saarland, Germany), mGluR5$^{loxp/loxp}$ (B6.129-Grm5 < tm1.1Jixu > /J) from Margarita Behrens (Salk institute for biological studies, La Jolla, California, USA), PGC1$\alpha^{loxp/loxp}$ from Jackson Lab (B6N.129(FVB)-Ppargc1a < tm2.1Brsp > /J) and td-Tomato$^{loxp/loxp}$ from Jackson Lab (AI14, B6.Cg-Gt(ROSA)26Sor m14(CAG-tdTomato)Hze/J). Mice used were C57BL/6J background. For astrocyte specific PGC-1α and mGluR5 deletion, hGFAPcre^{ERT} were bred with td-Tomato$^{loxp/loxp}$, PGC1$\alpha^{loxp/loxp}$ or mGluR5$^{loxp/loxp}$ with mice from an in-house colony (Figure S4A). For FACS experiments hGFAP-CFP mice were used. All experiments except for the immunohistochemistry were performed with male mice.

METHOD DETAILS

Maintenance, breeding and genotyping

All animal studies were approved by the « Service de la consommation et des affaires vétérinaries du Canton Vaud ». Mice were group housed with littermates in standard housing on a 12:12 h light/dark cycle. hGFAPcre^{ERT2}(B6.Tg(GFAP-cre/ERT2)1Fki), hGFAP-ECFP (TgN(hGFAP-ECFP)-GCED) have been obtained from Frank Kirchhoff (Molecular Physiology, University of Saarland, Germany), mGluR5$^{loxp/loxp}$ (B6.129-Grm5 < tm1.1Jixu > /J) from Margarita Behrens (Salk institute for biological studies, La Jolla, California, USA). PGC1$\alpha^{loxp/loxp}$ from Jackson Lab (B6N.129(FVB)-Ppargc1a < tm2.1Brsp > /J) and td-Tomato$^{loxp/loxp}$ from Jackson Lab (AI14, B6.Cg-Gt(ROSA)26Sor m14(CAG-tdTomato)Hze/J). Mice used were C57BL/6 background. The hGFAPcre^{ERT2} sequence was identified from phalange biopsies using the following primers: 5′- CAGGTTGGAGAGGAGACGCATCA-3′, 5′-CGTTGCATCGAC CGGTAATGCAGGC- 3′. The PGC$\alpha^{loxp/loxp}$ were identified with the following primers: 5′- TCCAGTAGGCAGAGATTTATGAC −3′, 5′- TGTCTGGTTTGACAATCTGCTAGG TC-3′ and mGluR5$^{loxp/loxp}$ were identified with the following primers: 5′- TTGCTAGCTGAAAAG GACGAAACA −3′, 5′- TCGTTTTGAATCTTGGGGGACAGTTAC- 3′. PCR reaction product coupled with syber green migrates in a 1,5% agarose gel then bands are revealed by UV lights. Mice were C57BL/6 background.

FACS of astrocytes and semiquantitative PCR

hGFAP-CFP, hGFAP-tdTomato and amGluR5cKO-tdTomato mice were used to purify CFP and tdTomato positive astrocytes. Frontal cortex were dissected from P3, P14, P20 or P50 old mice and samples were prepared as previously described (Buscemi et al., 2017; Boisvert et al., 2018). Briefly, CFP or tdTomato positive astrocytes were purified by fluorescence activated cell sorting (FACS) using a MoFlo AstriosEQ High speed cell sorter. Astrocytes were identified based on GFAP, ALDH1L and GLAST content (Figure S1C). Total RNA from sorted cells was isolated with RNeasy Mini Kit and the quantitative real-time PCR was done on C1000T Thermal Cycler as already described (Wall et al., 2002) (see Supplemental information for primer sequences).

Semiquantitative RT-PCR

Total RNA from sorted or harvested cells and tissue was isolated with RNeasy Mini Kit or Micro Kit (QIAGEN, 74104 or 74004) and RNA concentration was determined using a NanoDrop 1000 spectrophotometer (Witec AG, Switzerland). Reverse transcription was performed with 400-1000ng of DNase-treated total RNA using M-MLV reverse transcriptase (Promega, M3683). The quantitative real-time PCR was done on C1000T Thermal Cycler (CFX96 real-time PCR system, Bio-Rad) using SYBR Select Master Mix for CFX (Applied Biosystems – Life Technologies). The mRNA levels were normalized to the levels of β-actin, GAPDH or H3. The primer sequences used were the follows: PGC1α forward 5′-AGC CGT GAC CAC TGA CAA CGA G-3′, PGC1α reverse 5′-GCT CAT GGT

TCT GAG TGC TAA C-3′, PGC1β forward 5′-GGA CGC CAG TGA CTT TGA CT-3′, PGC1β reverse 5′-TTC ATC CAG TTC TGG GAA GC-3′, ESSRa forward 5′-AGG AAG CCC CGA TGG A-3′, ESSRa reverse 5′- GAG AGG CCT GGG ATG CTC TT-3′, ATP5a1 forward 5′-TCT CCA TGC CTC TAA CAC TCG-3′, ATP5a1 reverse 5′- CCA GGT CAA CAG ACG TGT CAG-3′, Cox4i forward 5′- ATT GGC AAG AGA GCC ATT TCT AC-3′, Cox4i reverse 5′- CAA CAC TCG CAT GTG CTC GAA-3′, Cox5b forward 5′- GGA AGA CCC TAA TCT AGT CCC C-3′, Cox5b reverse 5′- CCA CTA TTC TCT TGT TGC TGA-3′, Cycs forward 5′- AAA GGG AGG CAA GCA TAA GAC-3′, Cycs reverse 5′- GAA CAG ACC GTG GAG ATT TGG-3′, Ki67 forward 5′- AAT CCA ACT CAA GTA AAC GGG G-3′, Ki67 reverse 5′- TTG GCT TGC TTC CAT CCT CA-3′, GLT1 forward 5′- GGT CAT CTT GGA TGG AGG TC-3′, GLT1 reverse 5′- ATA CTG GCT GCA CCA ATG C-3′, Cx30 forward 5′- GGC CGA GTT GTG TTA CCT GCT-3, Cx30 reverse 5′- TCT CTT TCA GGG CAT GGT TGG-3′, Cx43 forward 5′- ACA GCG GTT GAG TCA GCT TG-3′, Cx43 reverse 5′- GAG AGA TGG GGA AGG ACT TGT-3′, Kir4.1 forward 5′- ATC AGA GCA GCC ACT TCA CC-3′, Kir4.1 reverse 5′- GGC TCT CTG TCT GAG TCG TC-3′, AldoA forward 5′- TGT TCT GCC TTA CAG ATC CTG G – 3′, AldoA reverse 5′- AAT GCG GTG AGC GAT GTC AG-3′, LDHA forward 5′- GCG TCT CCC TGA AGT CTC TT-3′, LDHA reverse 5′- AGC TTG ATC ACC TCG TAG GC-3′, TOP2A forward 5′-CCT CGG GGC AAA AGA GTC AT-3′, TOP2A reverse 5′-CTA TTC GTT GCC GGA GGC TT-3′; mGluR5 forward 5′- CTG CAC ACC TTG TAA GGA GAA TG-3′, mGluR5 reverse 5′- CAA ATC ACA ACC TGT CAA GTC-3′, H3 forward 5′- CTT CCA GCG TCG CCT CGG TC-3′; H3 reverse 5′-AGC GGT CTG CTT GGT TCG GG-3′; GAPDH forward 5′- TGC ACC ACC AAC TGC TTA GC- 3′, GAPDH reverse 5′- GGC ATG GAC TGT GGT CAT GAG – 3′β-actin forward 5′-GGCTGTATTCCCCTCCATCG-3′ β-actin reverse 5′-CCAGTTGGTAACAATGCCATGT-3′. For quantification ΔΔCT method was used.

In vivo treatments

(Z)-4-Hydroxytamoxifen (OH-TAM, Sigma-Aldrich, H7904) was used for the *in vivo* treatment from P5 to P12 (100mg/kg) daily, i.p. OH-TAM was dissolved in absolute ethanol and sunflower oil. To assess the proliferation of astrocytes, 5-bromo-2′-deoxyuridine (BrdU, Sigma-Aldrich) (50mg/kg) was administered i.p. daily during three days prior the brain collection.

Cell culture and treatment

Astrocyte cultures were prepared from cortices of 0- to 2- postnatal day (P0-P2) C57BL/6 (wild-type), hGFAPCre^{ERT2}R26-tdTomato-$^{loxp/loxp}$, hGFAPCre^{ERT2}PGC1α$^{loxp/loxp}$R26-tdTomato$^{loxp/loxp}$, hGFAPCre^{ERT2}mGluR5$^{loxp/loxp}$R26-tdTomato$^{loxp/loxp}$ pups, as previously described with some modifications (Marchaland et al., 2008; Prada et al., 2011; Bezzi et al., 1998). Briefly, dissociated cells were plated into 24 or 96 wells or Seahorse plates (180'000, 60'000 and 30'000 cells/well respectively) or in 25mm^2 flasks and maintained in a minimum essential medium (MEM, GIBCO, 21090-022) supplemented with Fetal Bovine Serum (FBS), 10%, PAA cell culture company, A15-101), L-glutamine (2mM, GIBCO, 25030-024), D-glucose (8mM), penicillin/streptomycin (100U/mL, 100μg/ml, GIBCO, 15140-22) and BHB (1mM, Sigma-Aldrich) during the first days. Cells were kept at 37°C in humidified 5%CO_2/95% air. In some experiments, cells were treated for 2 days since DIV5 with mPEP hydrochloride (1μM, R&D Systems), for 7 days since DIV3 with (Z)-4-Hydroxytamoxifen (OH-TAM, Sigma-Aldrich, H7904) (1 μM) and overnight with 15 ng/p24 mL of LentiPGC1α.

Metabolic assays

ATP measurements in primary astrocytes were obtained using ATP determination kit (Life Technologies). Cells were homogenized in lysis buffer (1% Triton X-100, 150mM NaCl, 10mM Tris-HCl, 5mM EDTA) supplemented with protease cocktail inhibitor, Complete (Roche) and centrifuged at 10,000xg for 5 minutes (min). The supernatant was collected and measured using the fluorescence plate reader GLOMAX (Promega). Lactate was measured using an L-Lactate assay kit (MAK065, Sigma). The medium was replaced with FBS-free medium, after 1h of incubation, the medium was collected and centrifuged at 10,000xg for 5 min. Cells were homogenized in lysis buffer (1% Triton X-100, 150mM NaCl, 10mM Tris-HCl, 5mM EDTA) supplemented with protease cocktail inhibitor, Complete (Roche) and centrifuged at 10,000xg for 5 min. The L-lactate from supernatant and from medium was colorimetrically determined by an absorbance measurement at 570 nm. The samples were normalized to the protein content.

Real-time measurements of OCR and ECAR were performed using an XFp Extracellular Flux Analyzer (Seahorse Bioscience, North Billerica, MA, USA). FACS-sorted astrocytes have been immobilised with CellTak (BD Biosciences) in the sensor cartridges (Seahorse Bioscience; 500,000 cells/well) immediately after the sorting procedure and then kept in non-buffered assay medium (KHB with 25 mM glucose, 1 mM sodium pyruvate, 2 mM glutamine for the measurement of ECAR, or 2.5 mM glucose and 1.5 mM carnitine for the measurement of OCR, pH 7) and incubated in a non-CO_2 incubator for 30 min at 37°C before analysis. Cells were plated in XF-96 plates (Seahorse Bioscience) at the concentration of 30'000 cells per well and cultured in DMEM medium supplemented with 5% FBS. OCR was measured in XF media (DMEM medium, containing 10 mM glucose, 2 mM L-glutamine and 1 mM sodium pyruvate), under basal conditions and in response to 2.5 μM oligomycin, 1.5 μM of carbonylcyanide-4-(trifluoromethoxy)-phenylhydrazone (FCCP) and 1 μM of Antimycin and Rotenone. Indices of mitochondrial respiratory function were calculated from OCR profile: basal OCR (before addition of oligomycin), ATP-linked OCR (calculated as the difference between basal OCR rate and oligomycin-induced OCR rate) and maximal OCR (calculated as the difference of FCCP rate and antimycin+rotenone rate). ECAR was measured in XF media in basal condition and in response to 10 mM glucose, 2.5 μM oligomycin and 100 mM of 2-DG (all from Sigma-Aldrich). Indices of glycolytic pathway activation were calculated from ECAR profile: basal ECAR (after the addition of glucose), maximal ECAR (after

the addition of oligomycin) and glycolytic capacity (calculated as the difference of oligomycin-induced ECAR and 2-DG-induced ECAR). Experiments with the Seahorse system were performed with the following assay conditions: 3-min mixture; 3-min wait; and 3-min measurement.

Immunocytochemistry

Cultured astrocytes were briefly washed with phosphate buffered saline (PBS) 1X and fixed with PFA 4% at 4°C for 10 min. After three washes with PBS1X cells were incubated for 1h at room temperature (RT) in PBS1X containing 4% of normal goat serum and Saponine (0.5mg/mL, Sigma-Aldrich, 47036) and then immunolabeled 2h at RT in PBS containing 4% of normal goat serum using the following primary antibodies: mouse-GS (Millipore, MAB302, 1:1000), mouse-GFAP (Millipore, MAB3402, 1:500) and rabbit- Ki67 (Abcam, ab15580, 1/500). After the incubation of primary antibodies, coverslips were washed three times with PBS1X and incubated during 2h at RT with fluorescent secondary antibodies (AlexaFluor, Invitrogen, Jackson ImmunoResearch, goat anti-mouse 488 and 555; goat anti-rabbit 488 and cy3; 1:300) diluted in PBS1X. Finally, nuclei were counterstained with 4', 6-diamidino-2-phenylindole (DAPI) (Invitrogen, 1:10000) and then washed before mounting with the FluorSave™ reagent (Merck-Millipore).

Tissue preparation, immunohistochemistry and analysis

hGFAP-tdTomato, aPGC1αcKO-tdTomato and amGluR5cKO-tdTomato mice were deeply anesthetized with sodium pentobarbitone (6mg/100 g body wt, i.p.) and immediately perfused intracardially with fresh 4% paraformaldehyde (pH 7.4) as already described (Buscemi et al., 2017). Brains were postfixed overnight at 4°C. Coronal sections (60 μm) were cut using a vibratome (VT1200S) and stored at 4°C in PBS1X supplemented with 0.02% sodium azide. BrdU detection required a prior DNA denaturation for 45min in 2M HCL at RT. For immunohistochemistry analysis sections were permeabilized for 45min in PBS1X containing 0.3% Triton X-100 and 15% normal goat or donkey serum and then immunolabeled overnight or 3 overnight at 4°C using the following primary antibodies: mouse-GS (Millipore, MAB302, 1:1000), mouse-NeuN (Millipore, MAB377, 1:200), guinea pig-VGLUT1 (Synaptic System, 135304, 1:1000), rabbit-VGLUT2 (Synaptic System, 135403, 1:500), mouse-PSD95 (Millipore, MAB1596, 1:600), rat-BrdU (Abcam, ab6326, 1:200), rabbit-cleaved Casp3 (BioConcept, 9664S, 1:400), rat-CTIP2 (Abcam, ab18465, 1:250), rabbit-NG2 (Abcam, ab5320, 1:250) and mouse-s100β (Abcam, anS2532, 1:1000). After primary antibody incubation brain sections were washed three times with PBS1X for 10min and incubated for 1.5h at RT with fluorescent secondary antibodies (AlexaFluor, Jackson ImmunoResearch, Invitrogen, goat anti-mouse 488, cy5; goat anti-rabbit 488, donkey anti-rat 488 and goat anti-guinea pig 488 and goat anti-mouse cy3; 1:300) diluted in PBS1X. Finally, nuclei were counterstained with DAPI (Invitrogen, 1:10000) and then washed before mounting with FluorSave™ reagent (Merck-Millipore).

Optical Sections were acquired every 0.4/0.6-μm, and confocal images were analyzed using Imaris (Bitplane AG, Zurich, Switzerland), Adobe Photoshop CS5 (Adobe System Incorporeted, San José, California, USA) or Fiji/ImageJ (NIH, USA) softwares. Astrocytic domains from L2/3 and L5 of the mPFC were used for analysis. All confocal images for Imaris (Bitplane AG, Zurich, Switzerland) analysis were taken with a high magnification, 63x-objective oil-immersion lens using Leica TCS SP5 or SP8 confocal microscopes. The volume and the morphological analysis of astrocytes, were performed by using original confocal Z stack images in Imaris Bitplane software. The individual analyzing the images was always blinded to the experimental conditions. Co-localization between PSD95 and VGLUT1 or VGLUT2 was calculated with the Leica software. Puncta were considered co-localized if the distance between them was $\leq$ 0.5 μm. Number of co-localized puncta was obtained and compared between the experimental groups.

Western blot analysis

Cultured astrocytes were treated with buffer or mPEP (10 μM, 30 min), BAPTA-AM (50 μM, 30 min), KN93 (10 μM, 30 min) or Rapamycin (100 nM, 30min). Following the treatments, DHPG (50 μM, 15min) was added. All the treatments were directly given in the culture medium. After treatments, cells were washed 2 times with ddH_2O and then lysis buffer (containing 10mM TrisHCl, 150 mM NaCl, 5 mM EDTA, 1% Triton X-100, 1% sodium deoxycholate, 1% phosphoSTOP™ (Roche), and a protease inhibitor cocktail (Sigma)) was added. Cells were detached with the help of a cell scraper, collected and sonicated. Cell lysates were centrifuged for 10 min, 12′000 rpm at 4°C. The supernatant containing the proteins was collected and quantified with the Bradford assay. Proteins were boiled for 5 min and separated on a denaturating 8% acrylamide gel. The following primary antibodies were used: mTOR (Mouse, Cell Signaling, 4517 1:2000), P-mTOR (Ser2448) (Rabbit, Cell Signaling, 2971, 1:2000), PGC1α (Mouse, Millipore, ST1202, 1:1000) and α- Tubulin (Mouse, Santa Cruz, SC-8085, 1:2000). The following secondary were used: goat-anti-rabbit, goat-anti-mouse, coupled with IRdye 800 or IRdye 680 (Li-Cor, Lincoln, 1:10.000). Protein bands were revealed by the Odyssey infrared image system (Li-Cor). Proteins were normalized with β-Tubulin.

Mitochondria staining and analysis

Cultured astrocytes. In order to visualize mitochondrial morphology, MitoTracker™ (100nM, Thermo Fisher) was added in culture media of cultured astrocytes and incubated for 15 min at 37°C. Astrocytes and mitochondria were visualized and images acquired using a Leica TCS SP5 confocal microscope (objective 63X, NA1.4**).** ***In utero electroporation.*** A mix of endotoxin-free plasmid preparation (PiggyBac transposase, 1μg/μL and PBmTAGBFP2_P2a_mtYFP, 1μg/μL) and 0.4% Fast Green (Sigma) was injected into lateral ventricle of one hemisphere of E15.5 embryos using Picospritzer® III (Parker Instrumentation. Electroporation (ECM830, BTX, Harvard Apparatus) was performed with platinum disk electrodes (Sonidel Limited) to target cortical progenitors by placing

the positively charged electrode on the side of DNA injection. Five pulses of 35V for 50ms with 500ms interval were used for electroporation. At the right postnatal age, animals were sacrificed by terminal perfusion of 4% PFA and collected as described before ("Tissue preparation"). ***Mitochondrion and astrocyte analysis.*** Mitotracker or mitoYFP (mitochondria) and BFP2 or tdTomato-expressing cells (astrocyte cytosol) were analyzed by acquiring serial z stacks (0.6/0.8 μm steps) of individual astrocytes within PFC tissue using an SP5 laser scanning confocal system (Leica) with a 63X objective (NA 1.4) for cultured cells and an SP8 laser scanning confocal system (Leica) with a 63X objective (NA 1.4) for tissue. The acquired stacks were transformed to surfaces (3D reconstruction) using Imaris (9.1, Bitplane AG, Zurich, Switzerland) and the "new surface" option by selecting the region of interest around a single astrocyte and adjusting the threshold (without background subtraction) in such a way as to avoid creating surfaces over noise and ensures that everything considered real fluorescence was covered by a gray surface The information concerning mitochondrial or astrocyte volume, and mitochondrial volume and sphericity was exported in Excel files. The volume and sphericity of all of the quantified mitochondria (typically in the range of several hundreds) per astrocyte were plotted using Excel and OriginPro software (OriginLab), and the resulting diagrams were used to quantify the percentage of fragmented versus tubular mitochondria per astrocyte, using a sphericity cut-off value of 0.3. At least 8-10 astrocytes per mouse were analyzed, and the percentage of all of the individual astrocytes from the same mouse were pooled. The images and the 3D reconstruction were exported and adjusted using Adobe Photoshop CS5 (Adobe System Incorporated, San José, California, USA) or Fiji/ImageJ (NIH, USA) software.

Lentiviral vector production

A pENTR222 plasmid containing fluorescent reporters GFP or DsRed or the mouse PGC1α with a FLAG epitope at the 5′ end was generated (Geneart, Invitrogen, Life Technologies, Zug, Switzerland). The lentiviral vector SIN-cPPT-GfaABC1DB(3)-mouse FLAG-PGC1-alpha-WPRE-miR124T(N) was obtained with a Gateway LR Clonase® reactions (Invitrogen, Life Technologies, Zug, Switzerland; SIN-cPPT-GfaABC1DB(3)-Gateway-WPRE-miR124T(N) plasmid (Merienne et al., 2013). The VSV-G pseudotyped lentiviral vector was produced as previously described (Hottinger et al., 2000). The batch was aliquoted in PBS, 1% BSA and frozen at 80°C. The final viral concentration was calculated by the p24 ELISA assay (RETROtek, Kampenhout, Belgium; 388 ng p24 antigen/μl).

Stereotaxic intracranial delivery of viral vector

Mice (P5) were anesthetized using isoflurane at 5% (w/v), placed in a small animal stereotaxic frame (David Kopf Instruments) and maintained at 0.5%–2.0% isoflurane (w/c) for the duration of surgery. Pinch reflexes were regularly tested to confirm anesthetic depth. After exposing the skull, a small hole was drilled in the skull overlying the prefrontal cortex (AP + 1.2/1.3 mm, L ± 0.2/0.3 mm and DV −0.9/1.3mm). LentiPGC-1α was injected (0.5 μL total volume for site) bilaterally or unilaterally through Hamilton syringe at a rate of 100 nL min^{-1} using CMA400 Pump (CMA System). Following IUE, LentiPGC1α was injected (0.5 μL total volume) in the electroporated area. After surgical procedures, mice were returned to their home cage with the mother.

Acute brain slice preparation

Mice were briefly anesthetized with isoflurane and decapitated. The brain was quickly removed and transferred to ice-cold solution containing (in mM) 65 NaCl, 2.5 KCl, 1.25 NaH_2PO_4, 25 $NaHCO_3$, 7 $MgCl_2$, 0.5 $CaCl_2$, 25 glucose, and 105 sucrose saturated with 95% O_2 and 5% CO_2; 350-μm-thick coronal slices containing the mPFC were cut from the tissue block with a vibratome (HM 650, Microm). Slices were then transferred to a recovery solution containing (in mM) 130 K-gluconate, 15 KCl, 0.2 EGTA, 20 HEPES, 25 glucose for 2 min before being kept in oxygenated artificial cerebrospinal fluid (ACSF, 315 mOsm) saturated with 95% O_2 and 5% CO_2 and containing (in mM) 125 NaCl, 2.5 KCl, 1.25 NaH_2PO_4, 25 $NaHCO_3$, 1 $MgCl_2$, 2 $CaCl_2$, and 25 glucose at 34°C for 25 min and then at RT until use.

Recordings of miniature excitatory post-synaptic currents

Whole-cell patch-clamp recordings were performed in the soma of layer 5 pyramidal cells in the mPFC. Individual slices were put in a recording chamber with oxygenated ACSF at a flow rate of 1 to 2 mL/min. All electrophysiology experiments were done at 32-34°C. Images were acquired with Retiga R1 camera using Ocular software (Qimaging, Germany) with a 40x water immersion objective. Recordings were performed using Multiclamp 700B amplifier and data were acquired with a Digidata 1550A 16-bit board (all from Molecular Devices). For miniature EPSCs, Somata were patched with borosilicate glass pipettes (2.5-4 MΩ) containing in mM: 130 gluconic acid, 130 CsOH, 5 CsCl, 10 HEPES, 1.1 EGTA, 10 Na-phosphocreatine, 4 Mg-ATP, 0.3 Na-GTP. The pH was adjusted to 7.3 with CsOH, and 1.5 $mg.ml^{-1}$ biocytin was added for the reconstruction of neurons. Cells were voltage clamped at −70 mV and synaptic responses were recorded in the presence of picrotoxin (100 μM) and TTX (1 μM). Recordings with unstable baseline or greater than −400 pA were rejected. Currents were filtered offline using a Butterworth low-pass filter (2 kHz) and analyzed in 1 min bins using the Mini-Analysis Program 6.0.7 (Synaptosoft Inc., USA). Recordings with leak increasing more than 100 pA and access resistance (< 15 MΩ) changing more than 30% between the beginning and the end of the recording were discarded. At least 100 events were analyzed for any condition. Events were identified as miniature excitatory post-synaptic currents (mEPSCs) by setting the event detection threshold at least 2-fold the baseline noise level and by checking that events had (i) rise times faster than the decay time, (ii) rise times greater than 0.5 ms, and (iii) decay times greater than 1.5 ms. Events not fitting the above parameters were rejected. Event amplitudes, inter-event intervals, rise and decay times were first averaged within each experiment and regrouped by condition. The resulting means were averaged between experiments. Single cell properties (access resistance,

membrane capacitance, etc.) were analyzed with Clampfit 10.5 (Axon instruments, Union City, CA). Graphs were done using Graphpad prism and Illustrator 15.1.0 (Adobe). Reagents for ACSF and internal solutions, biocytin and picrotoxin were obtained from Sigma-Aldrich while TTX was obtained from Tocris. Picrotoxin was dissolved in EtOH and TTX was dissolved in ddH_2O

Biocytin labeling

Internal solutions used for somatic L5 pyramidal cells patch-clamp experiments contained biocytin (1.5 $mg.ml^{-1}$) that diffused in the cells for at least 10 minutes. Slices (350 μm) containing the recorded cell were then immersion-fixed in 4% PFA at 4°C overnight. The following day, slices were washed in PBS 274 mM NaCl before being transferred to blocking solution containing 10% NGS in 0.3% Triton-PBS 274 mM NaCl for 1 hour. Afterward, for the immunochemical staining, slices were put in blocking solution containing Alexa Fluor 488-conjugated streptavidin (1:700, Jackson ImmunoResearch Europe Ltd, code: 705-546-147) for 2 hours. Slices were then washed three times for 10 minutes each in PBS containing 274 mM NaCl before being mounted on superfrost plus microscope slides. Images were acquired on a Zeiss LSM710 Pascal confocal microscope through a 0.9 NA × 10 Plan-apochromat objective and the ZEN2012 software (Carl Zeiss). Whenever applicable, contrast and illumination were adjusted in ImageJ. Presented images are Z projections.

QUANTIFICATION AND STATISTICAL ANALYSIS

All analysis were performed using GraphPad Prism 8.0.2 software. One-way and Two-way ANOVA were performed followed by Bonferroni's multiple comparison test. For two simple comparisons, unpaired t test was used. All data are presented as mean ± SEM and replicate information is indicated in the figure legends.